

Riquiqui and Minibrain are regulators of the Hippo pathway downstream of Dachshous

Joffrey L. Degoutin^{1,2}, Claire C. Milton^{1,2,3}, Eefang Yu^{1,2}, Marla Tipping⁴, Floris Bosveld⁵, Liu Yang⁴, Yohanns Bellaïche⁵, Alexey Veraksa⁴ and Kieran F. Harvey^{1,2,3,6}

The atypical cadherins Fat (Ft) and Dachshous (Ds) control tissue growth through the Salvador–Warts–Hippo (SWH) pathway, and also regulate planar cell polarity and morphogenesis. Ft and Ds engage in reciprocal signalling as both proteins can serve as receptor and ligand for each other. The intracellular domains (ICDs) of Ft and Ds regulate the activity of the key SWH pathway transcriptional co-activator protein Yorkie (Yki). Signalling from the FtICD is well characterized and controls tissue growth by regulating the abundance of the Yki-repressive kinase Warts (Wts). Here we identify two regulators of the *Drosophila melanogaster* SWH pathway that function downstream of the DsICD: the WD40 repeat protein Riquiqui (Riq) and the DYRK-family kinase Minibrain (Mnb). Ds physically interacts with Riq, which binds to both Mnb and Wts. Riq and Mnb promote Yki-dependent tissue growth by stimulating phosphorylation-dependent inhibition of Wts. Thus, we describe a previously unknown branch of the SWH pathway that controls tissue growth downstream of Ds.

The SWH pathway has been theorized to control organ size on the basis of the fact that modulation of pathway activity influences the size of both *D. melanogaster* and murine organs^{1–4}. Deregulation of SWH pathway activity has also been linked to carcinogenesis in humans^{1,5}. The best-defined receptor for the SWH pathway is the large atypical cadherin Ft (refs 6–10), which is activated by binding to its ligand, the related cadherin Ds (refs 11,12). Both Ft and Ds possess several extracellular cadherin repeats and cytoplasmic tails that mediate intracellular signalling events^{4,13,14}. Ds acts not only as a ligand for Ft but also functions as a receptor that signals through its ICD to regulate planar cell polarity (PCP), morphogenesis and SWH pathway activity^{11,14–20}. For example, the DsICD is required for *D. melanogaster* imaginal disc cells to derepress Yki activity in response to ectopic *ds* expression¹¹. In addition, in a *ds* mutant background, *dsICD* overexpression activates Yki and causes tissue overgrowth in a cell-autonomous fashion¹⁸. Ft is likely to act as a ligand for Ds because Ds is partially required for overexpression of the Ft extracellular domain (ECD) to trigger Yki hyperactivation¹⁸. Therefore, Ds can both promote Yki activity cell-autonomously, and repress Yki activity non-cell-autonomously by signalling through Ft.

The mechanism by which Ft mediates cell-autonomous repression of Yki has been extensively studied^{4,13,21}. The Four-jointed (Fj)

kinase regulates the interaction between the ECDs of Ft and Ds (refs 22–24). On binding to Ds on neighbouring cells, Ft controls imaginal disc growth through downstream proteins including the atypical myosin Dachs¹⁰, the LIM-domain protein Zyxin²⁵ and the palmitoyltransferase Approximated²⁶. These proteins influence the activity of the SWH pathway core kinase cassette, by regulating the abundance of the Wts kinase^{10,25}. Wts in turn represses tissue growth by phosphorylating and inhibiting the Yki transcriptional co-activator protein²⁷. Ft also controls the stability and subcellular localization of Expanded (Ex; refs 6–8), another upstream regulator of the SWH pathway.

In contrast to signalling from the FtICD to the SWH pathway, signalling events downstream of the DsICD are poorly defined. DsICD regulates morphogenesis by polarizing Dachs¹⁴, and has been proposed to activate Yki by sequestering SWH pathway proteins at the apical membrane¹⁸. Here we describe the identification of a membrane-to-nucleus Ds signalling pathway that promotes Yki activity by repressing Wts. Unlike the Ft branch of the SWH pathway, Ds-mediated regulation of Wts and Yki occurs independently of Dachs. In contrast, Ds promotes Yki activity by signalling through the WD40 repeat protein Riq and the DYRK family kinase Mnb to induce phosphorylation-mediated repression of Wts.

¹Cell Growth and Proliferation Laboratory, Peter MacCallum Cancer Centre, 7 St Andrews Place, East Melbourne, Victoria 3002, Australia. ²Sir Peter MacCallum Department of Oncology, University of Melbourne, Parkville, Victoria 3010, Australia. ³Department of Pathology, University of Melbourne, Parkville, Victoria 3010, Australia. ⁴Department of Biology, University of Massachusetts Boston, Boston, Massachusetts 02125, USA. ⁵Polarity, Division and Morphogenesis Team, Institut Curie, CNRS UMR 3215, INSERM U934, 26 Rue d'Ulm, 75248 Paris Cedex 05, France.

⁶Correspondence should be addressed to K.F.H. (e-mail: kieran.harvey@petermac.org)

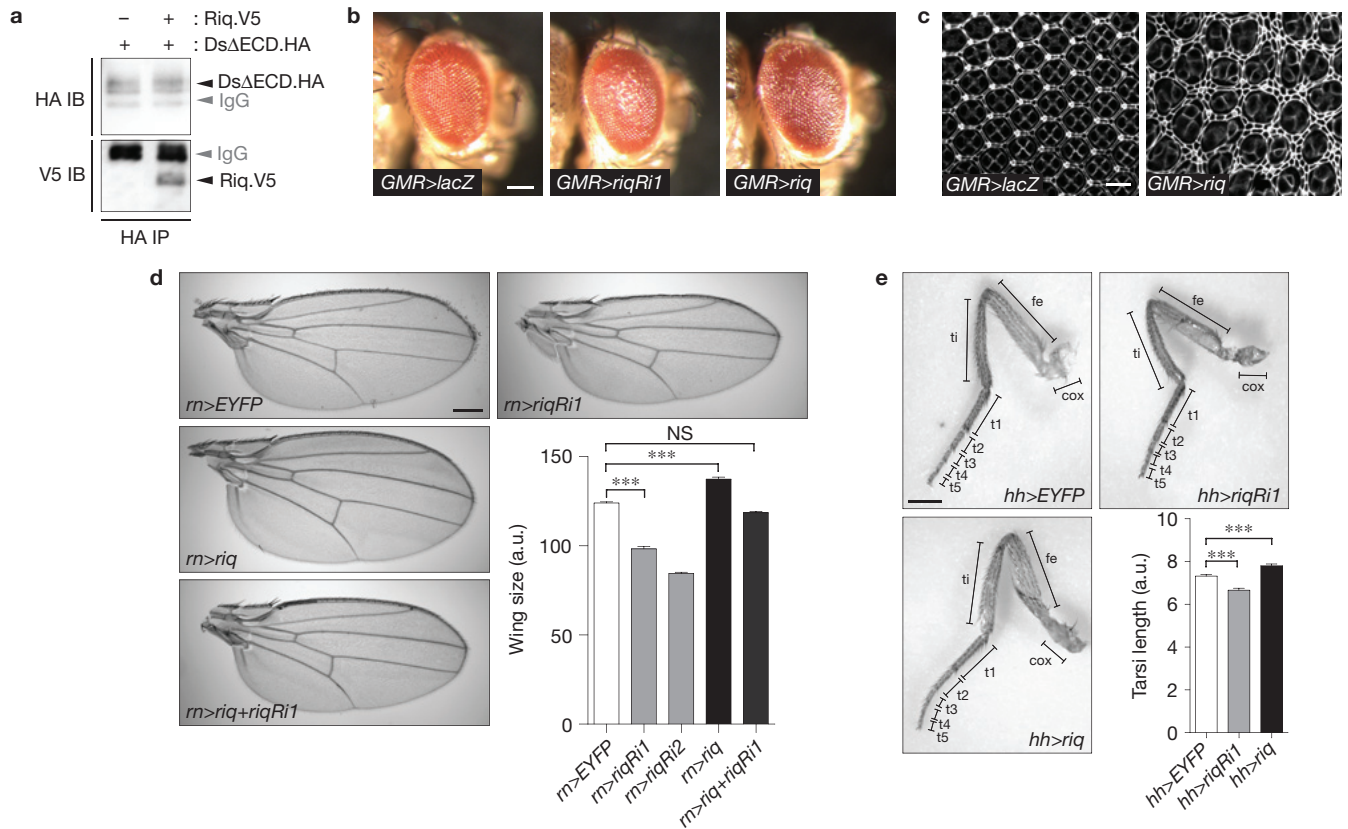


Figure 1 Riq forms a physical complex with Ds and controls tissue growth. **(a)** Lysates from S2 cells transfected with Ds Δ ECD.HA, alone or in combination with Riq.V5, were immunoprecipitated (IP) with anti-HA antibodies. Western blots (IB) were performed using anti-HA and anti-V5 antibodies to reveal Ds and Riq, respectively. **(b)** Lateral views of adult female eyes (anterior is to the right) expressing *UAS-lacZ*, *UAS-riqRi1* or *UAS-riq* under the control of *GMR-Gal4*. **(c)** Eyes 44 h after puparium formation expressing *UAS-lacZ* or *UAS-riq* under the control of *GMR-Gal4* that have been stained with anti-Ds-large antibody. **(d)** Wing area from adult female flies expressing *UAS-EYFP*, *UAS-riqRi1*, *UAS-riqRi2*, *UAS-riq*

or *UAS-riqRi1* concomitantly with *UAS-riq* under the control of *rn-Gal4*. Representative images are shown and wing size was quantified for each genotype ($n = 20$ for each). **(e)** Right rear legs from adult female flies expressing *UAS-EYFP*, *UAS-riqRi1* or *UAS-riq* under the control of *hh-Gal4*. Leg segments are as follows: coxa (cox), femur (fe), tibia (ti) and tarsal segments 1 to 5 (t1, t2, t3, t4, t5). The length of the entire tarsal segment was quantified ($n = 15$ for each genotype). In **d, e**, data are presented as mean \pm s.e.m.; *** $P < 0.001$; NS, not significant; a.u., arbitrary units. Scale bars: 100 μ m (**b**), 10 μ m (**c**) and 200 μ m (**d, e**). Uncropped images of blots are shown in Supplementary Fig. S8.

RESULTS

Riq, a newly identified Ds-interacting protein

To investigate the growth control function of Ds we attempted to identify proteins that signal downstream of the DsICD by using affinity purification in *D. melanogaster* S2 cells and mass spectrometry²⁸. An abundant Ds-interacting protein was the uncharacterized protein CG14614, hereafter referred to as Riq, referring to its small size phenotype, as described below. Riq is a 343-amino-acid protein and contains five WD40 repeats predicted to mediate protein–protein interactions. Riq homologues are present throughout the animal kingdom and in plants, and are highly conserved; *D. melanogaster* Riq and its human homologue (DCAF7) are 85% identical and 91% similar. The zebrafish Riq homologue Wdr68 has been implicated in craniofacial development²⁹, but Riq has not been studied *in vivo* in other organisms. To confirm Riq as a Ds-interacting protein we performed immunoprecipitation experiments using transfected S2 cell lysates. As shown in Fig. 1a, a robust physical interaction was detected between Riq and the DsICD (Ds Δ ECD). Further, Ds was required for the Riq protein to localize to the apical junction of wing imaginal disc epithelial

cells, and expression of Ds Δ ECD recruited a proportion of Riq to S2 cell membranes (Supplementary Fig. S1).

Riq regulates tissue growth

To investigate a potential role for Riq in tissue growth, we modulated its expression in the developing eye, wing and leg with independent *riq* RNA interference (RNAi) transgenes and UAS-inducible *riq* transgenes. A slight decrease in adult eye size was observed when *UAS-riq* RNAi was expressed using *GMR-Gal4*, compared with control eyes expressing a *UAS-lacZ* transgene (Fig. 1b). Conversely, a modest increase in eye size was observed when *riq* was overexpressed using *GMR-Gal4*. Consistently, *riq* overexpression caused an increase in interommatidial cell number in pupal eye discs 44 h after puparium formation (Fig. 1c).

We further explored a role for Riq in tissue growth by modulating its expression in developing wings using *rotund-Gal4* (*rn-Gal4*). RNAi-mediated depletion of Riq caused a 21% or 32% decrease in wing size depending on the RNAi line used (Fig. 1d). Conversely, *riq* overexpression caused an 11% increase in wing size. The observed reduction in wing size was due to Riq depletion as *riq* transgene

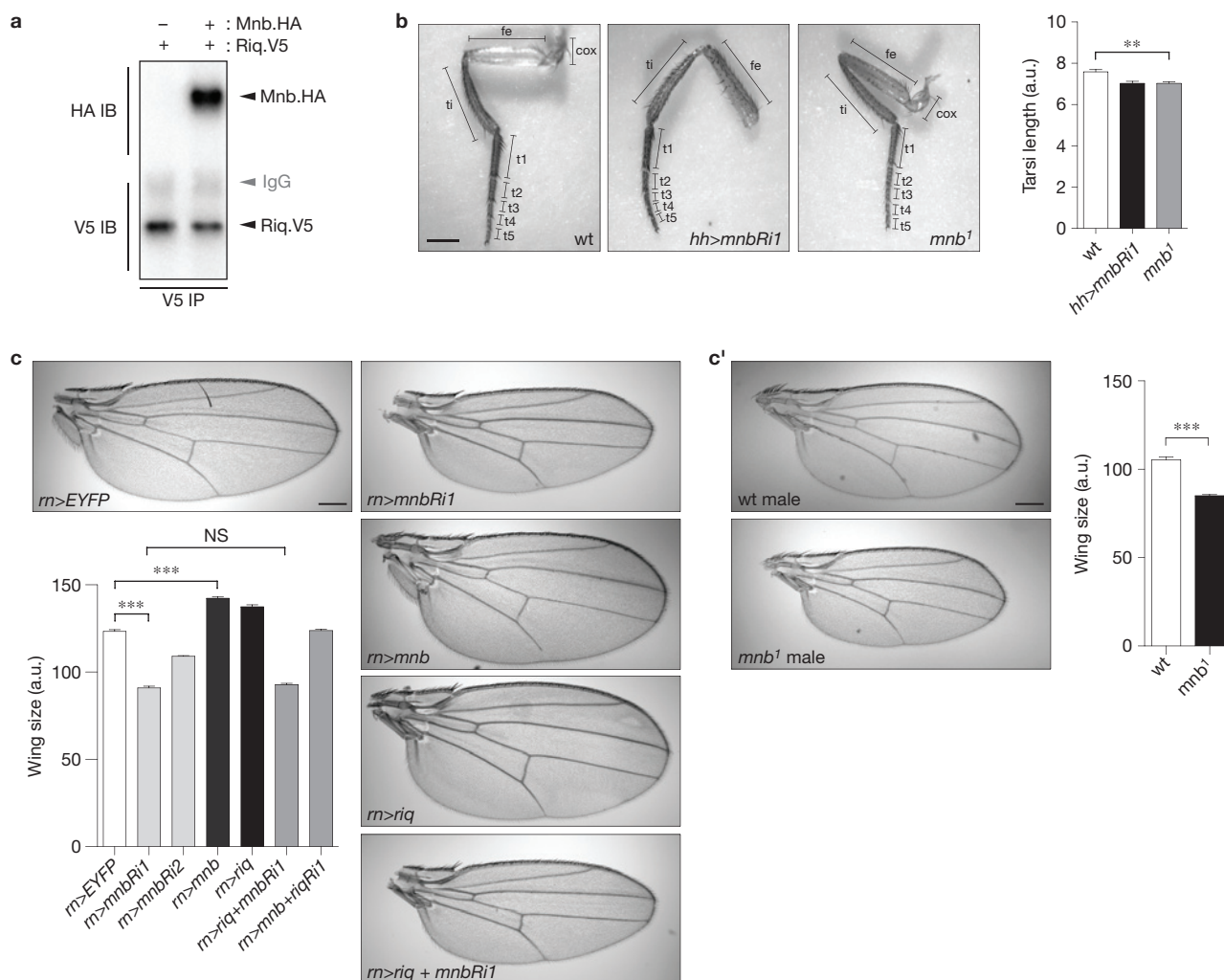


Figure 2 Mnb physically interacts with Riq and phenocopies its effect on tissue growth. **(a)** Lysates from S2 cells transfected with Riq.V5 alone, or together with Mnb.HA, were immunoprecipitated with anti-V5 antibodies. Western blots were performed using anti-HA and anti-V5 antibodies to reveal Mnb and Riq, respectively. **(b)** Images of right rear legs from adult female flies expressing *hh-Gal4*-driven *UAS-EYFP* or *UAS-mnbRi1*, or legs from *mnb¹* flies. The entire tarsal segment of individual legs was quantified ($n = 15$ for each genotype). Leg segments are as follows: coxa (cox), femur (fe), tibia (ti) and tarsal segment 1 to 5 (t1, t2, t3, t4, t5). **(c)** Wing area from adult female flies expressing

UAS-EYFP as control, *UAS-mnbRi1*, *UAS-mnbRi2*, *UAS-mnb*, *UAS-riq*, *UAS-mnbRi1* concomitantly with *UAS-riq* or *UAS-mnb* concomitantly with *UAS-riqRi1* under the control of *rn-Gal4*. Representative images are shown and wing size was quantified ($n = 20$ for each genotype). **(c')** Area of adult male wings of *mnb¹* mutant flies were quantified and compared with adult wild-type male wings. Representative images are shown. Results from leg and wing quantification (**b,c,c'**) are presented as mean \pm s.e.m., *** $P < 0.001$, ** $P < 0.01$; NS, not significant. Scale bars, 200 μ m. Uncropped images of blots are shown in Supplementary Fig. S8.

expression rescued this size reduction (Fig. 1d). Further, expression of *riq* RNAi reduced expression of endogenous Riq in wing discs, as determined using an antibody against the human Riq homologue DCAF7 and by real-time PCR (Supplementary Fig. S2a,b). Modulation of Riq expression using *hedgehog-Gal4* (*hh-Gal4*) also affected leg size; legs expressing *riq* RNAi were 9% shorter, whereas *riq* overexpression increased leg length by 7% (Fig. 1e). Collectively, these data suggest that Riq regulates the size of wings, eyes and legs.

The Mnb kinase forms a physical complex with Riq and is functionally related

The human Riq homologue DCAF7 physically complexes with the human DYRK1A kinase (homologous to *D. melanogaster* Mnb)³⁰.

Given the high degree of conservation of Riq, we investigated the possibility that Riq and Mnb physically and functionally interact. Initially, we tested whether Riq and Mnb physically interact by performing co-immunoprecipitation experiments on S2 cell lysates expressing epitope-tagged versions of Mnb and Riq. As shown in Fig. 2a, a robust physical association was observed between Riq and Mnb.

Subsequently, we investigated a potential role for Mnb in leg and wing growth. The length of tarsal segments of legs from flies expressing a *mnb* RNAi transgene or *mnb¹* hemizygous flies (which express 60% to 70% less Mnb protein than wild-type flies)³¹ was in each case 7% smaller than in control flies (Fig. 2b). Expression of independent *mnb* RNAi lines with *rn-Gal4* caused a significant reduction in adult wing size (Fig. 2c). Consistent with a role for Mnb as a growth-promoting

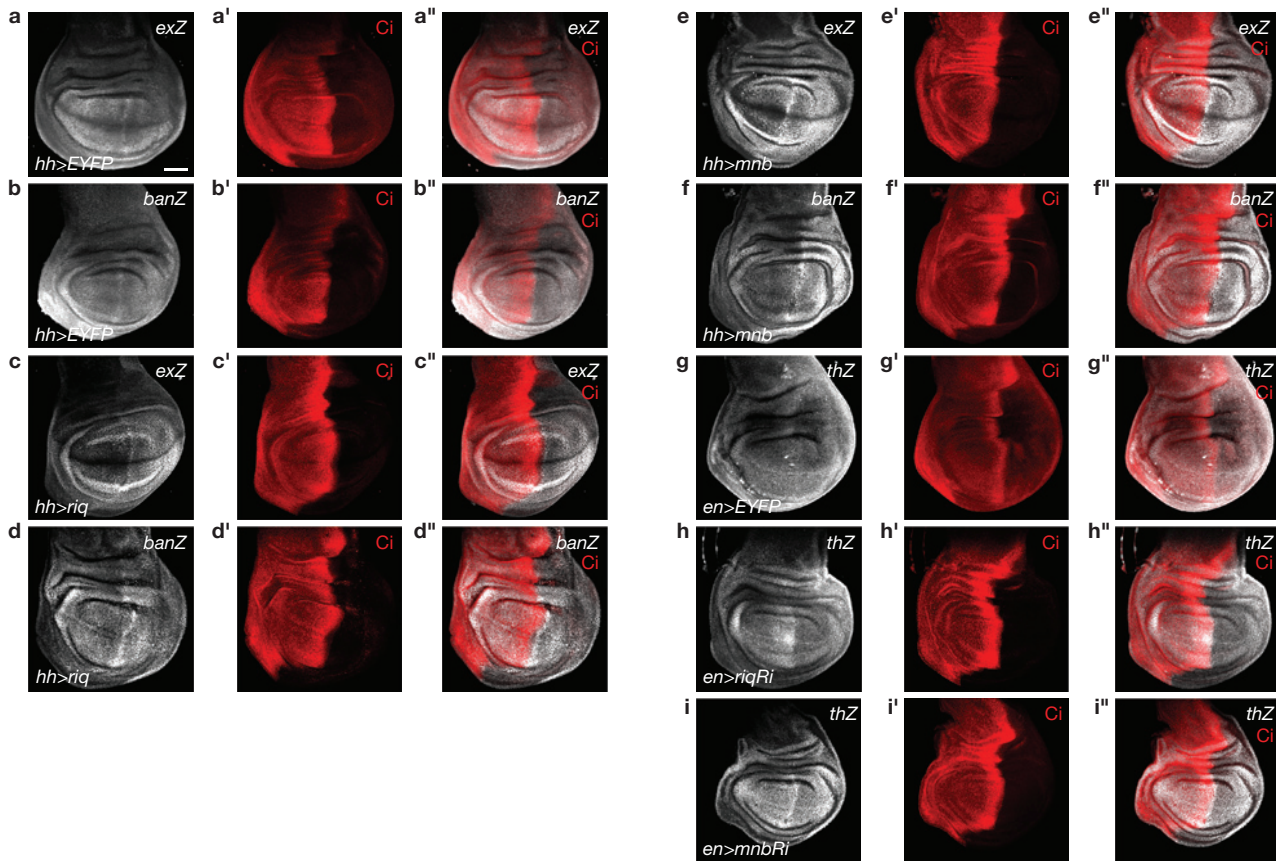


Figure 3 Riq and Mnb regulate SWH pathway activity. (a–i) Wing imaginal discs (anterior is to the left) from third instar *D. melanogaster* larvae harbouring the following elements: *hh-Gal4*, *UAS-EYFP* and *ex-lacZ* (a); *hh-Gal4*, *UAS-EYFP* and *ban-lacZ* (b); *hh-Gal4*, *UAS-riq* and *ex-lacZ* (c); *hh-Gal4*, *UAS-riq* and *ban-lacZ* (d); *hh-Gal4*, *UAS-mnb* and *ex-lacZ* (e); *hh-Gal4*, *UAS-mnb* and *ban-lacZ* (f); *en-Gal4*, *UAS-EYFP* and *th-lacZ* (g);

en-Gal4, *UAS-riqRi* and *th-lacZ* (h); and *en-Gal4*, *UAS-mnbRi* and *th-lacZ* (i). Yki activity (grey in a–i) was reported by *ex-lacZ* (a,c,e), *ban-lacZ* (b,d,f) or *th-lacZ* (g–i). All transgenes were expressed in the posterior compartment of wing imaginal discs; *Cubitus interruptus* (Ci) expression (red in a'–i') marks the anterior compartment. Merged images are shown in (a''–i''). Scale bar, 50 μ m.

protein, *rn-Gal4*-driven *mnb* overexpression led to a 15% increase in wing size (Fig. 2c). Further, *mnb¹* flies possessed wings that were 19% smaller than wild-type flies (Fig. 2c'). These findings suggest that Mnb, like Riq, is required for normal wing and leg growth.

To begin to assess whether Mnb and Riq control wing size together we used *rn-Gal4* to simultaneously overexpress Riq, and deplete Mnb by RNAi. Mnb depletion completely suppressed the ability of Riq to promote wing overgrowth as these wings were undergrown and were of a similar size to wings expressing *mnb* RNAi alone (Fig. 2c). In the converse experiment, Riq depletion partially suppressed the ability of *mnb* overexpression to induce wing overgrowth (Fig. 2c). Collectively, our biochemical and genetic data support a model whereby Riq and Mnb function together to promote tissue growth.

Riq and Mnb regulate activity of the SWH pathway oncoprotein Yki

Ds has been postulated to control SWH pathway activity by acting both as a receptor and ligand for Ft (refs 11,15,18). On the basis of our above data, we reasoned that Riq and Mnb control tissue growth downstream of the DsICD by modulating SWH pathway activity. To address this hypothesis we modulated expression of Mnb and Riq and assessed

Yki activity using *lacZ* enhancer traps in the *ex*, *thread* (*th* or *Diap1*) and *bantam* (*ban*) genes. Both *riq* and *mnb* overexpression caused Yki activity to increase, as indicated by increases in *ex-lacZ*, *th-lacZ* or *ban-lacZ* when compared with the control posterior compartment, and to control wing imaginal discs that did not overexpress *riq* or *mnb* (Fig. 3a–f and Supplementary Fig. S3). Occasionally, increased Yki activity was observed at the anterior/posterior border of wing imaginal discs expressing Riq or Mnb, although we are unsure of its significance. Consistent with our findings above, RNAi-mediated depletion of either Riq or Mnb led to reduced Yki activity, as determined by *th-lacZ* (Fig. 3g–i). Collectively, these experiments suggest that Riq and Mnb regulate tissue growth by controlling Yki activity.

Riq, Mnb and Wts physically interact with each other

Ft controls SWH pathway activity by regulating the localization and abundance of Dachs at the apical junction of epithelial cells¹⁰, and Ds polarizes Dachs to regulate morphogenesis¹⁴. However, we found no evidence that Ds controls tissue growth through Dachs, as modulating the expression of either Riq or Mnb did not influence Dachs levels or localization in wing imaginal discs or the pupal notum, and these proteins seemed to control wing size in parallel (Supplementary Fig. S4).

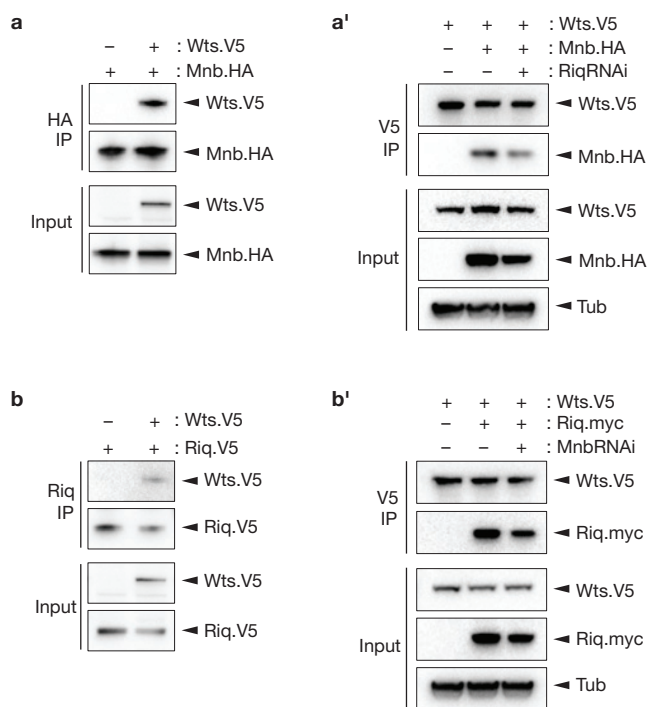


Figure 4 Riq and Mnb physically interact with Wts. (**a–b'**) S2 cells were transfected with the indicated plasmids. In **a'** V5-tagged Wts was expressed alone or together with HA-tagged Mnb in the presence or absence of dsRNA specific for Riq. In **b'** V5-tagged Wts was expressed alone or together with Myc-tagged Riq in the presence or absence of dsRNA specific for Mnb. 48 h post transfection, immunoprecipitations were performed as follows: (**a,a',b,b'**) using anti-HA antibodies (**a**); using anti-V5 antibodies (**a'**); using anti-DCAF7 antibodies (human homologue of Riq; **b**); using anti-V5 antibodies (**b'**). Subsequently, immunoprecipitates and input lysates were subjected to SDS–PAGE and western blots were performed using antibodies to Myc, HA, V5 or tubulin. Uncropped images of blots are shown in Supplementary Fig. S8.

To further investigate how Mnb and Riq regulate the SWH pathway we used biochemical approaches. Given that Mnb is a kinase, we reasoned that it interacts with and phosphorylates a component(s) of the SWH pathway. To test this notion we co-expressed Mnb and Riq with select SWH pathway proteins in S2 cells and determined whether they formed a physical complex using immunoprecipitations. Interestingly, we found that both Riq and Mnb physically interacted with Wts (Fig. 4a,b and Supplementary Fig. S5a). The ability of Mnb to physically interact with Wts was not obviously dependent on Riq, as in cells treated with Riq double-stranded RNA (dsRNA), Mnb still immunoprecipitated with Wts (Fig. 4a'). A similar result was observed when Wts and Riq were immunoprecipitated in the presence or absence of Mnb dsRNA (Fig. 4b'). These results suggest that Mnb and Riq are not essential for each other's ability to interact with Wts.

Riq and Mnb repress the SWH pathway by phosphorylating and inhibiting the Wts kinase

In parallel, we sought to determine whether Mnb phosphorylates Wts. When co-expressed with Mnb the mobility of Wts was decreased (Fig. 5a), whereas Hippo (Hpo) and Salvador (Sav) mobility were unaffected (Supplementary Fig. S5c). Riq alone did not obviously affect Wts mobility but potentiated the ability of Mnb to alter Wts

Table 1 Mnb phosphorylates six amino acids in the Wts protein, including a DYRK1A consensus site.

Phosphorylation site	Wts1 peptide
Thr 59	R.NDALT*PDYHHAK.Q
Ser 146	R.CS*PALDSGAGSSR.S
Thr 173	R.T*VGNPGGNGGFSPSPSGFSEVAPPAPPPR.N
Ser 184	R.TVGNPGGNGGF*S*PSPSGFSEVAPPAPPPR.N
Ser 227	K.RRS*PALNNRPPAIPPTQR.G
Ser 246	R.GNS*PVITQNLK.N

Wts amino acids that were phosphorylated by Mnb, but not Mnb K386R, as detected by mass spectrometry are shown, as well as the digested peptides that were phosphorylated.

mobility (Fig. 5a). The influence of Mnb on Wts mobility was also observed when these proteins were co-expressed with Sav and Hpo, known regulators of Wts phosphorylation (Fig. 5b).

To investigate whether the observed change in Wts mobility was the result of phosphorylation, we generated a kinase-dead version of Mnb by mutating its ATP-binding site (Mnb K386R). Co-expression of Mnb K386R with Wts failed to modify Wts mobility in the presence or absence of Riq (Fig. 5c). In addition, Mnb-induced changes in Wts mobility were reversed when lysates were treated with calf intestinal phosphatase before electrophoresis (Fig. 5d). Together, these data show that Mnb-dependent alteration of Wts mobility is caused by phosphorylation. We also investigated whether Homeodomain-interacting protein kinase (Hipk) could alter the mobility of Wts because Hipk is the closest Mnb homologue in *D. melanogaster*, its human orthologue (HIPK2) can also physically interact with the human Riq orthologue (DCAF7; ref. 32), and we and others found that Hipk regulates tissue growth through the SWH pathway^{33,34}. However, in contrast to Mnb, Hipk had no effect on Wts mobility, suggesting that it regulates SWH pathway activity by an alternative mechanism to Mnb (Supplementary Fig. S5d).

We then explored which region of Wts was phosphorylated by Mnb by expressing three portions of the Wts protein, with or without Mnb. Only Wts1, representing amino acids 1–318, showed a clear mobility change in the presence of Mnb (Fig. 5e,f), which was enhanced when Riq was also overexpressed (Fig. 5g). To determine whether Mnb could indeed phosphorylate this portion of Wts we performed *in vitro* kinase assays using immunoprecipitated Mnb or Mnb K386R, and recombinant GST–Wts1 as a substrate. After incubation in kinase buffer supplemented with [γ -³²P]ATP, Mnb, but not Mnb K386R, exhibited strong autophosphorylation confirming that the K386R mutation renders Mnb inactive. Mnb stimulated strong phosphorylation of GST–Wts1, whereas Mnb K386R did not (Fig. 5h). Further, Mnb failed to phosphorylate the negative control protein, GST–Calcyclin-binding protein (GST–CACYBP; Supplementary Fig. S5e).

To identify Wts residues that are phosphorylated by Mnb, we digested *in vitro* kinase assays with trypsin and analysed them by mass spectrometry. In two independent experiments we identified six Wts residues that were phosphorylated in the presence of Mnb, but not Mnb K386R, and three of these were identified in each experiment (Table 1). Of note, one of these residues (Ser 246) is in a region that closely matches the consensus DYRK1A phosphorylation site (RPxS/TP; ref. 35, and is conserved between Wts and one of its vertebrate homologues (LATS1) in multiple species (Supplementary Fig. S6). Further, in unbiased global phosphoproteomic studies, this site is phosphorylated in both human LATS1 (refs 36,37) and *Drosophila* Wts (ref. 38).

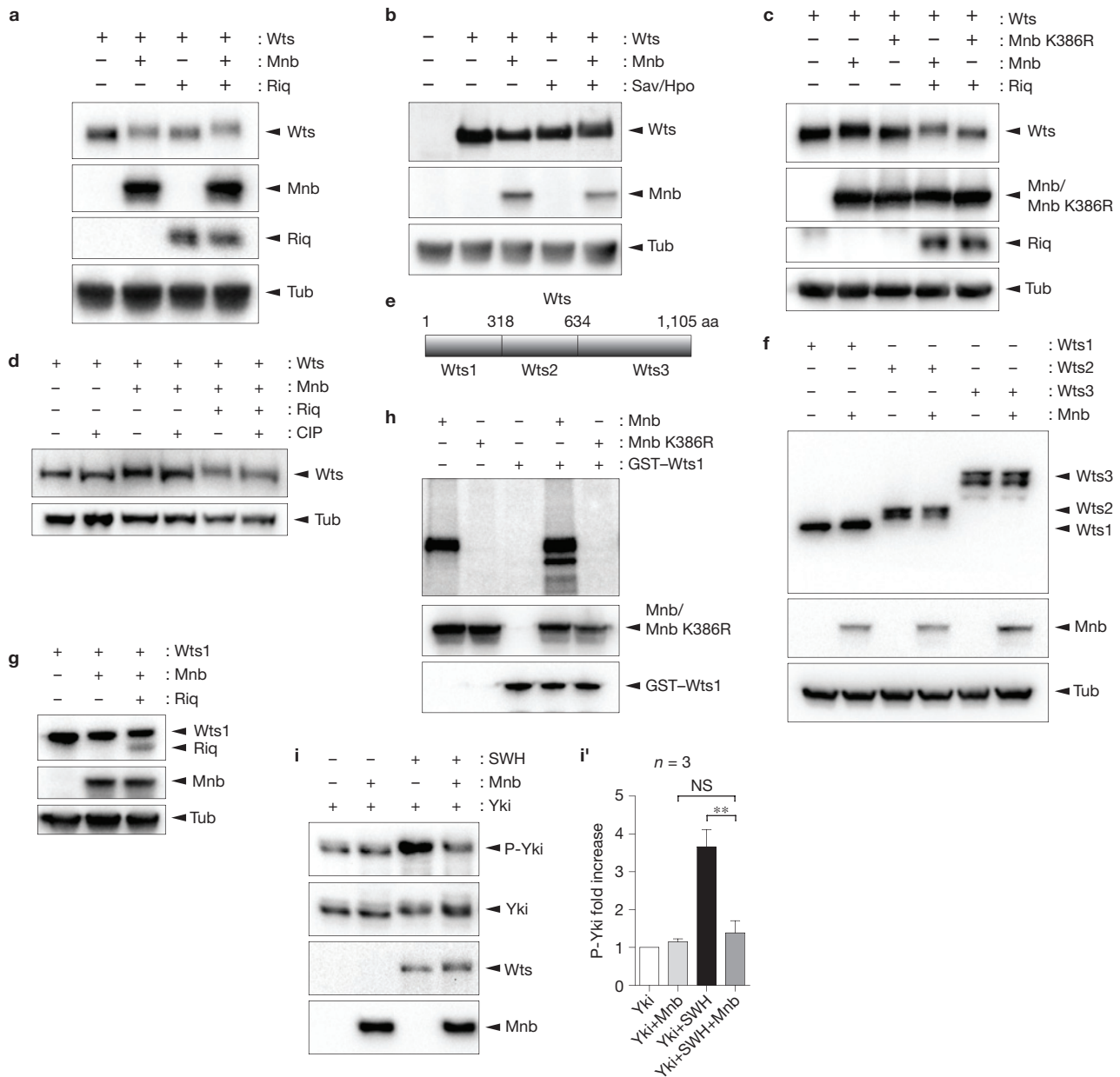


Figure 5 Mnb phosphorylates Wts and inhibits its activity. **(a–d)** Western blot analysis of lysates from S2 cells transfected with the indicated plasmids. Wts and Riq were revealed with anti-V5, and Mnb or Mnb K386R with anti-HA. Tubulin (Tub) levels were assessed to ensure even protein loading. Note that tubulin exhibited no change in mobility. In **d** some lysates were treated with calf intestinal phosphatase (CIP) before being subjected to SDS-PAGE. **(e)** Schematic diagram of the Wts protein and the fragments of Wts (Wts1, Wts2 and Wts3) that were expressed in S2 cells alone or together with Mnb. **(f,g)** Western blot analysis was performed with antibodies against V5 (to reveal Wts and Riq), HA (to reveal Mnb) and tubulin. **(h)** Kinase assays performed using recombinant GST-Wts1 as a

substrate and either Mnb or Mnb K386R immunoprecipitated from S2 cells. Isolated proteins were incubated alone or together in kinase buffer containing [γ - 32 P]ATP and subjected to SDS-PAGE (upper panel). Western blotting was used to detect input proteins (lower panels). **(i)** Yki was expressed alone, with Sav, Wts and Hpo (SWH), or Mnb together SWH in S2 cells. Yki phosphorylation was assessed by western blotting using an anti-phospho-S168-Yki antibody. **(i')** Fold increase of phospho-Yki/total Yki derived from three independent experiments was quantified. ** $P < 0.01$; NS, not significant. Uncropped images of blots are shown in Supplementary Fig. S8. Statistics source data for Fig. 5i' are available in Supplementary Table S1.

Next, we investigated the functional consequence of Mnb-dependent phosphorylation of Wts. On the basis of our observations that Riq and Mnb normally promote tissue growth and Yki activity, we reasoned that Riq and Mnb repress Wts activity. Wts stimulates phosphorylation of Yki on at least three residues, with Ser 168 being the main site^{39,40}.

Co-expression of Mnb with Yki did not influence basal phosphorylation of Yki at Ser 168, as detected by a phospho-Yki-S168 antibody (Fig. 5i). In the presence of Sav, Wts and Hpo (SWH), or Mnb together SWH in S2 cells, Yki was strongly phosphorylated at Ser 168; when quantified across three independent experiments, a 3.7-fold increase was observed (Fig. 5i'). When Mnb was expressed

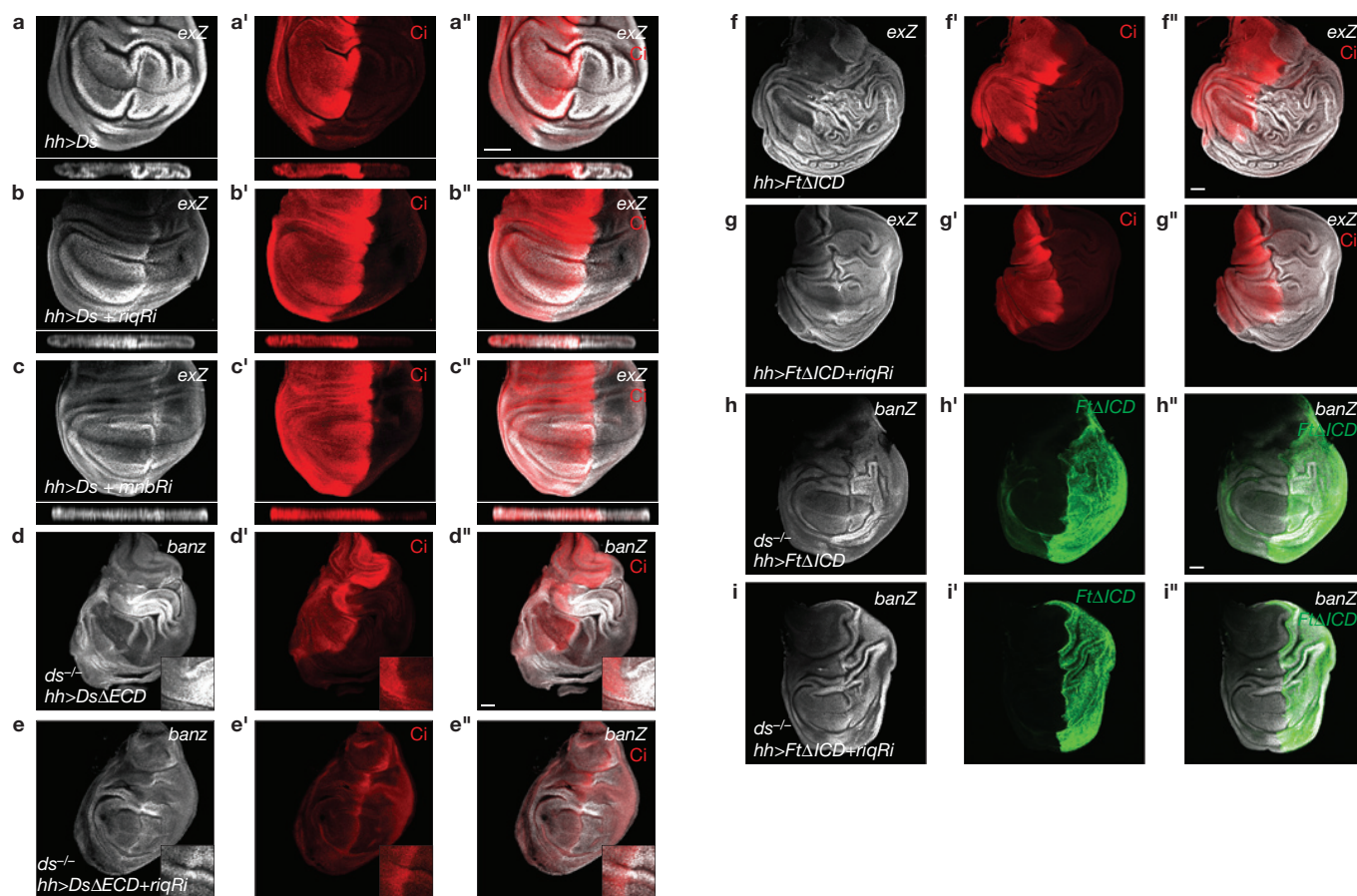


Figure 6 Riq and Mnb function downstream of Ds to promote Yki activity. (a–i) Wing imaginal discs from third instar *D. melanogaster* larvae harbouring the following elements: *hh-Gal4*, *UAS-ds* and *ex-lacZ* (a); *hh-Gal4*, *UAS-ds*, *UAS-riqRi* and *ex-lacZ* (b); *hh-Gal4*, *UAS-ds*, *UAS-mnbRi* and *ex-lacZ* (c); *hh-Gal4*, *UAS-dsΔECD*, and *ban-lacZ* in a *ds* mutant organism (d); *hh-Gal4*, *UAS-dsΔECD*, *UAS-riqRi* and *ban-lacZ* in a *ds* mutant organism (e); *hh-Gal4*, *UAS-ftΔICD* and *ex-lacZ* (f); *hh-Gal4*, *UAS-ftΔICD*, *UAS-riqRi* and *ex-lacZ* (g); *hh-Gal4*,

UAS-ftΔICD, and *ban-lacZ* in a *ds* mutant organism (h); *hh-Gal4*, *UAS-ftΔICD*, *UAS-riqRi* and *ban-lacZ* in a *ds* mutant organism (i). Yki activity was reported by *ex-lacZ* or *ban-lacZ* levels (grey in a–i). Ci expression (red in a'–g') marked the anterior compartment whereas HA-FtΔICD expression (green in h',i') marked the posterior compartment, of wing imaginal discs. Merged images are shown in a''–i''. X–Z sections through the wing pouch are shown below planar sections of wing discs in a–c''. Scale bars, 50 μm.

together with Sav, Wts and Hpo, the level of Yki-S168 phosphorylation was reduced when compared with that observed in cells expressing Sav, Wts and Hpo but not Mnb (Fig. 5i,i'). Mnb did not repress Wts activity by modulating its abundance as depletion of neither Mnb, nor Riq, by RNAi affected Wts expression (Supplementary Fig. S5f). These data show that Mnb represses Wts and are consistent with the idea that Riq and Mnb promote tissue growth by de-repressing Yki.

Riq and Mnb activate Yki downstream of Ft/Ds binding

To determine whether Riq and Mnb function downstream of the Ds/ICD to regulate the ability of Wts to limit Yki activity, we performed experiments in developing *D. melanogaster* tissues similar to those described in Fig. 3. We first overexpressed *ds* in the posterior compartment of wing imaginal discs using *hh-Gal4* and found that Yki activity, as assessed by *ex-lacZ*, was increased, especially in the wing pouch (Fig. 6a). The previously reported finding that *ds* overexpression induces non-cell-autonomous increases in Yki activity provided an assay to investigate whether Riq functions downstream of the Ds/ICD to regulate Yki (Fig. 6a; ref. 18). Consistent with this, *ex-lacZ* levels

in the posterior *dsICD*-expressing domain of the wing disc were greatly reduced when either Riq or Mnb was depleted by RNAi, but non-cell-autonomous Yki hyperactivation in anterior cells near the AP boundary was unaffected (Fig. 6b–c''). Mnb and Riq depletion also suppressed Ds-induced effects on wing disc morphology (X–Z sections in Fig. 6a–c). Suppression of Ds-induced Yki activation was not caused by reduced Ds expression as depletion of neither Mnb nor Riq affected Ds levels (Supplementary Fig. S7).

A potential complicating factor in the above experiment is that Ft and Ds engage in reciprocal regulation of the SWH pathway^{11,18}. To test this we performed a similar experiment as above, but used a Ds construct consisting only of its ICD (*DsΔECD*) that cannot engage with Ft (ref. 41). We also performed this experiment in *ds* mutant animals to avoid potential effects associated with endogenous Ds. In agreement with previous findings¹⁸, we observed strong Yki hyperactivation (as assessed by *ban-lacZ*) and tissue overgrowth, particularly in the hinge region of imaginal discs (Fig. 6d). RNAi-mediated depletion of Riq substantially suppressed Yki hyperactivity and morphological defects caused by *dsΔECD* expression (Fig. 6e).

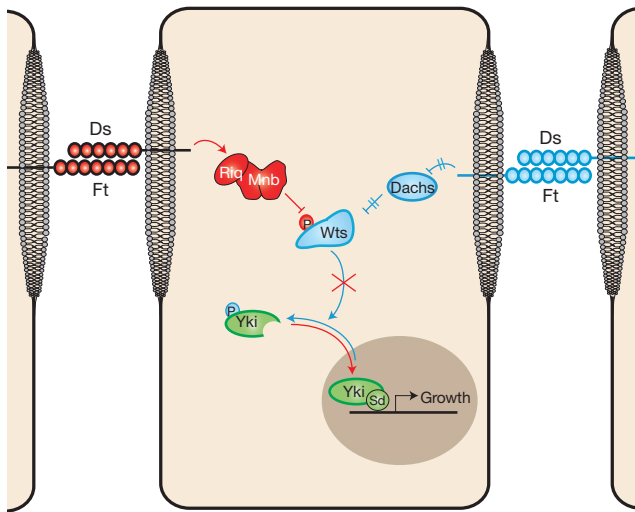


Figure 7 Model of signalling from Ds and Ft to the SWH pathway. Signalling from the DsICD is represented in red (positively regulating growth) and signalling from the FtICD in blue (negatively regulating growth). Sd, Scalloped.

Consistent with the idea that signalling downstream of the DsICD regulates Yki activity in response to Ds–Ft binding, expression of the FtECD (*ftΔICD*) can hyperactivate Yki in a Ds-dependent fashion¹⁸. To determine whether Ds-dependent activation of Yki requires Riq and Mnb, we overexpressed *ftΔICD* in the posterior compartment of wing discs and assessed Yki activity in the absence or presence of *riq* RNAi. *ftΔICD* expression strongly increased *ex-lacZ* and caused substantial overgrowth and folding of the posterior wing disc (Fig. 6f). RNAi-mediated depletion of Riq in *ftΔICD*-expressing tissues partially suppressed both of these phenotypes (Fig. 6g).

Overexpression of *ftΔICD* can stimulate Yki activity even in *ds* mutant animals (Fig. 6h), possibly by having a dominant-negative effect on endogenous Ft (ref. 18). If Riq regulates Yki activity specifically in response to Ft–Ds binding and signalling downstream of the DsICD, we reasoned that Riq would be dispensable for Yki hyperactivity in tissues that overexpressed *ftΔICD* but lacked Ds. To test this, we repeated the above experiment in a *ds* mutant background and found that, indeed, Riq RNAi had no impact on Yki hyperactivity in *ftΔICD*-expressing tissues in the absence of Ds (Fig. 6i). Collectively, these data show that in response to Ft–Ds binding, the DsICD promotes Yki-dependent tissue growth by signalling through Riq (Fig. 7).

DISCUSSION

The related cadherins Ft and Ds control tissue growth by regulating SWH pathway activity^{6–8,10–12}, and also control PCP and morphogenesis^{13–15,42}. Intriguingly, Ft and Ds regulate SWH pathway activity by engaging in reciprocal signalling as a ligand–receptor pair. Signalling downstream of Ft is reasonably well defined, but signalling downstream of Ds in growth control has remained uncharacterized until the discovery of a membrane-to-nucleus signalling pathway controlling SWH pathway activity downstream of the DsICD, described here. Our genetic and biochemical data imply that the WD40 repeat protein Riq complexes with the DsICD and can bind to the Mnb and Wts kinases. Riq promotes Mnb-dependent phosphorylation and

inhibition of Wts, and thereby promotes Yki-dependent tissue growth. Further investigation is required to define biologically relevant Wts residues that are phosphorylated by Mnb. Our study shows that Mnb phosphorylates Wts on several residues in its amino-terminal third, although it is formally possible that other regions of Wts are also phosphorylated by Mnb.

Therefore, Ds–Ft ligation induces two seemingly opposing growth-regulatory events: Ds activates Ft, which represses Yki by modulating Dachs^{11,12}; whereas Ft signals through Ds, Riq and Mnb to activate Yki. At first glance it seems counter-intuitive that Ft–Ds binding would both promote, and repress Yki-dependent tissue growth but raises several interesting possibilities. One option is that the timing of signalling from both the DsICD and the FtICD is different and varies throughout the cell cycle. For example, DsICD might deliver a pulse of Yki activity to induce transcriptional events associated with tissue growth. Subsequently, to ensure that Yki activity does not perdure and cause tissue overgrowth, it could be repressed by signalling from FtICD. Alternatively, DsICD or FtICD signalling might predominate over the other in different regions of imaginal discs or at different stages of development, to regulate Yki. How such regulation could occur is unclear, but could possibly: stem from polarized activity of Ft and Ds that occurs in cells of growing imaginal discs in response to graded expression of Ds and Ft (refs 23,24); occur if the influence of signalling downstream of FtICD or DsICD on Wts activity was quantitatively different; result from non-uniform activity of additional proteins that mediate Ft and Ds signalling. Alternatively, repression of Yki by the FtICD, and activation by the DsICD, could quantitatively oppose each other and serve to set a fine threshold of Yki activity that is highly sensitive to regulation by other branches of the SWH pathway such as the Kibra–Ex–Merlin complex^{43–46}, the Hpo activating kinase Tao-1 (refs 47,48) or apical polarity proteins^{49–52}. In future studies it will be important to define the spatiotemporal activity profile of FtICD and DsICD signalling and the relative influence of the Ds and Ft branches of the SWH pathway on tissue growth.

Given that Ft and Ds also engage in bi-directional signalling to control PCP (ref. 17) and morphogenesis¹⁶, it will be important to determine whether Riq and Mnb control these processes downstream of the DsICD. In addition, it will be important to investigate whether the signalling events described here are conserved in mammals. Interestingly, a reverse regulatory event to that described here, between the human orthologues of Wts (LATS2) and Mnb (DYRK1A), has been reported. LATS2 was shown to phosphorylate DYRK1A and promote senescence of cultured cells⁵³, raising the possibility that Wts/LATS1/2 and Mnb/DYRK1A/1B kinases engage in mutual regulatory relationships.

Finally, given the emergence of the SWH pathway as an important regulator of different human tumours^{1,5}, the present study raises the possibility that in a pathological setting the human orthologues of Riq (DCAF7) and Mnb (DYRK1A and DYRK1B) could function as oncogenes. Cell culture studies have provided conflicting reports on whether *DYRK1A* and *DYRK1B* act as oncogenes or tumour suppressor genes^{53–59}. However, *in vivo* studies in both flies and mice, and genetic studies in humans, have described only positive roles for Mnb/DYRK1A/DYRK1B in tissue growth: *dyrk1a* heterozygous mice exhibit growth retardation and impaired brain development⁶⁰;

DYRK1A mutations cause microcephaly and growth retardation in humans^{61–63}; whereas Mnb promotes *D. melanogaster* tissue growth (this study and ref. 31). These *in vivo* studies support the possibility that DYRK1A, DYRK1B and DCAF7 could be oncogenic in human cancers. □

METHODS

Methods and any associated references are available in the [online version of the paper](#).

Note: Supplementary Information is available in the online version of the paper

ACKNOWLEDGEMENTS

We thank C. House for assistance with mass spectrometry, J. Lin and K. Hannan for expertise with kinase assays and S. Blair (University of Madison, Wisconsin, USA), I. Edery (Rutgers University, USA), C. House (Peter MacCallum Cancer Centre, Australia), K. Irvine (Rutgers University, USA), D. Pan (Johns Hopkins University, USA), M. Simon (Stanford University, USA), D. Strutt, University of Sheffield, UK), N. Tapon (Cancer Research UK, UK), F. Tejedor (Universidad Miguel Hernandez, Spain), K. Yu (Korea Research Institute of Bioscience and Biotechnology), the Developmental Studies Hybridoma Bank, the Vienna *Drosophila* RNAi Center, the Australian *Drosophila* Research Support Facility (www.ozdros.com), the National Institute of Genetics and the Bloomington Stock Centre for fly stocks, plasmids and antibodies. K.F.H. is a Sylvia and Charles Viertel Senior Medical Research Fellow. This research was supported by a Project Grant from the National Health and Medical Research Council of Australia, and by NIH grants GM097727 and CA156734 and NSF grant 0640700 to A.V. Mass spectrometry was performed at the Taplin Facility, Harvard Medical School, USA and Bio21, University of Melbourne, Australia.

AUTHOR CONTRIBUTIONS

J.L.D. and C.C.M. performed *Drosophila* genetic experiments. J.L.D. and E.Y. carried out biochemistry and molecular biology experiments. M.T., L.Y. and A.V. performed affinity purification and mass spectrometry. F.B. and Y.B. analysed Dachs localization in the pupal notum. J.L.D. and K.F.H. designed experiments, analysed data and wrote the manuscript.

COMPETING FINANCIAL INTERESTS

The authors declare no competing financial interests.

Published online at www.nature.com/doi/10.1038/ncb2829

Reprints and permissions information is available online at www.nature.com/reprints

- Harvey, K. & Tapon, N. The Salvador–Warts–Hippo pathway—an emerging tumour-suppressor network. *Nat. Rev. Cancer* **7**, 182–191 (2007).
- Badouel, C., Garg, A. & McNeill, H. Herding Hippo: regulating growth in flies and man. *Curr. Opin. Cell Biol.* **21**, 837–843 (2009).
- Halder, G. & Johnson, R. L. Hippo signaling: growth control and beyond. *Development* **138**, 9–22 (2011).
- Reddy, B. V. & Irvine, K. D. The Fat and Warts signaling pathways: new insights into their regulation, mechanism and conservation. *Development* **135**, 2827–2838 (2008).
- Harvey, K. F., Zhang, X. & Thomas, D. M. The Hippo pathway and human cancer. *Nat. Rev. Cancer* **13**, 246–257 (2013).
- Bennett, F. C. & Harvey, K. F. Fat cadherin modulates organ size in *Drosophila* via the Salvador/Warts/Hippo signaling pathway. *Curr. Biol.* **16**, 2101–2110 (2006).
- Willecke, M. *et al.* The fat cadherin acts through the hippo tumor-suppressor pathway to regulate tissue size. *Curr. Biol.* **16**, 2090–2100 (2006).
- Silva, E., Tsatskis, Y., Gardano, L., Tapon, N. & McNeill, H. The tumor-suppressor gene fat controls tissue growth upstream of expanded in the hippo signaling pathway. *Curr. Biol.* **16**, 2081–2089 (2006).
- Tyler, D. M. & Baker, N. E. Expanded and fat regulate growth and differentiation in the *Drosophila* eye through multiple signaling pathways. *Dev. Biol.* **305**, 187–201 (2007).
- Cho, E. *et al.* Delineation of a fat tumor suppressor pathway. *Nat. Genet.* **38**, 1142–1150 (2006).
- Willecke, M., Hamaratoglu, F., Sansores-Garcia, L., Tao, C. & Halder, G. Boundaries of Dachsous cadherin activity modulate the Hippo signaling pathway to induce cell proliferation. *Proc. Natl Acad. Sci. USA* **105**, 14897–14902 (2008).
- Rogulja, D., Rauskolb, C. & Irvine, K. D. Morphogen control of wing growth through the Fat signaling pathway. *Dev. Cell* **15**, 309–321 (2008).
- Sopko, R. & McNeill, H. The skinny on fat: an enormous cadherin that regulates cell adhesion, tissue growth, and planar cell polarity. *Curr. Opin. Cell Biol.* **21**, 717–723 (2009).
- Bosveld, F. *et al.* Mechanical control of morphogenesis by Fat/Dachsous/Four-jointed planar cell polarity pathway. *Science* **336**, 724–727 (2012).
- Lawrence, P. A., Struhl, G. & Casal, J. Do the protocadherins Fat and Dachsous link up to determine both planar cell polarity and the dimensions of organs? *Nat. Cell Biol.* **10**, 1379–1382 (2008).
- Clark, H. F. *et al.* Dachsous encodes a member of the cadherin superfamily that controls imaginal disc morphogenesis in *Drosophila*. *Genes Dev.* **9**, 1530–1542 (1995).
- Casal, J., Lawrence, P. A. & Struhl, G. Two separate molecular systems, Dachsous/Fat and starry night/frizzled, act independently to confer planar cell polarity. *Development* **133**, 4561–4572 (2006).
- Matakatsu, H. & Blair, S. S. Separating planar cell polarity and Hippo pathway activities of the protocadherins Fat and Dachsous. *Development* **139**, 1498–1508 (2012).
- Thomas, C. & Strutt, D. The roles of the cadherins Fat and Dachsous in planar polarity specification in *Drosophila*. *Dev. Dyn.* **241**, 27–39 (2012).
- Brittle, A., Thomas, C. & Strutt, D. Planar polarity specification through asymmetric subcellular localization of Fat and Dachsous. *Curr. Biol.* **22**, 907–914 (2012).
- Grusche, F. A., Richardson, H. E. & Harvey, K. F. Upstream regulation of the hippo size control pathway. *Curr. Biol.* **20**, R574–R582 (2010).
- Ishikawa, H. O., Takeuchi, H., Haltiwanger, R. S. & Irvine, K. D. Four-jointed is a Golgi kinase that phosphorylates a subset of cadherin domains. *Science* **321**, 401–404 (2008).
- Simon, M. A., Xu, A., Ishikawa, H. O. & Irvine, K. D. Modulation of fat: Dachsous binding by the cadherin domain kinase four-jointed. *Curr. Biol.* **20**, 811–817 (2010).
- Brittle, A. L., Repiso, A., Casal, J., Lawrence, P. A. & Strutt, D. Four-jointed modulates growth and planar polarity by reducing the affinity of dachsous for fat. *Curr. Biol.* **20**, 803–810 (2010).
- Rauskolb, C., Pan, G., Reddy, B. V., Oh, H. & Irvine, K. D. Zyxin links fat signaling to the hippo pathway. *PLoS Biol.* **9**, e1000624 (2011).
- Matakatsu, H. & Blair, S. S. The DHHC palmitoyltransferase approximated regulates Fat signaling and Dachs localization and activity. *Curr. Biol.* **18**, 1390–1395 (2008).
- Huang, J., Wu, S., Barrera, J., Matthews, K. & Pan, D. The Hippo signaling pathway coordinately regulates cell proliferation and apoptosis by inactivating Yorkie, the *Drosophila* homolog of YAP. *Cell* **122**, 421–434 (2005).
- Kyriakakis, P., Tipping, M., Abed, L. & Veraksa, A. Tandem affinity purification in *Drosophila*: the advantages of the GS-TAP system. *Fly (Austin)* **2**, 229–235 (2008).
- Nissen, R. M., Amsterdam, A. & Hopkins, N. A zebrafish screen for craniofacial mutants identifies wdr68 as a highly conserved gene required for endothelin-1 expression. *BMC Dev. Biol.* **6**, 28 (2006).
- Skurat, A. V. & Dietrich, A. D. Phosphorylation of Ser640 in muscle glycogen synthase by DYRK family protein kinases. *J. Biol. Chem.* **279**, 2490–2498 (2004).
- Tejedor, F. *et al.* minibrain: a new protein kinase family involved in postembryonic neurogenesis in *Drosophila*. *Neuron* **14**, 287–301 (1995).
- Ritterhoff, S. *et al.* The WD40-repeat protein Han11 functions as a scaffold protein to control HIPK2 and MEKK1 kinase functions. *EMBO J.* **29**, 3750–3761 (2010).
- Poon, C. L., Zhang, X., Lin, J. I., Manning, S. A. & Harvey, K. F. Homeodomain-interacting protein kinase regulates hippo pathway-dependent tissue growth. *Curr. Biol.* **22**, 1587–1594 (2012).
- Chen, J. & Verheyen, E. M. Homeodomain-interacting protein kinase regulates yorkie activity to promote tissue growth. *Curr. Biol.* **22**, 1582–1586 (2012).
- Himpel, S. *et al.* Specificity determinants of substrate recognition by the protein kinase DYRK1A. *J. Biol. Chem.* **275**, 2431–2438 (2000).
- Daub, H. *et al.* Kinase-selective enrichment enables quantitative phosphoproteomics of the kinome across the cell cycle. *Mol. Cell* **31**, 438–448 (2008).
- Dephousse, N. *et al.* A quantitative atlas of mitotic phosphorylation. *Proc. Natl Acad. Sci. USA* **105**, 10762–10767 (2008).
- Bodenmiller, B. *et al.* PhosphoPep—a phosphoproteome resource for systems biology research in *Drosophila* Kc167 cells. *Mol. Syst. Biol.* **3**, 139 (2007).
- Oh, H. & Irvine, K. D. *In vivo* regulation of Yorkie phosphorylation and localization. *Development* **135**, 1081–1088 (2008).
- Dong, J. *et al.* Elucidation of a universal size-control mechanism in *Drosophila* and mammals. *Cell* **130**, 1120–1133 (2007).
- Matakatsu, H. & Blair, S. S. Separating the adhesive and signaling functions of the Fat and Dachsous protocadherins. *Development* **133**, 2315–2324 (2006).
- Mao, Y. *et al.* Planar polarization of the atypical myosin Dachs orients cell divisions in *Drosophila*. *Genes Dev.* **25**, 131–136 (2011).
- Hamaratoglu, F. *et al.* The tumour-suppressor genes NF2/Merlin and Expanded act through Hippo signalling to regulate cell proliferation and apoptosis. *Nat. Cell Biol.* **8**, 27–36 (2006).
- Genevet, A., Wehr, M. C., Brain, R., Thompson, B. J. & Tapon, N. Kibra is a regulator of the Salvador/Warts/Hippo signaling network. *Dev. Cell* **18**, 300–308 (2010).
- Baumgartner, R., Poernbacher, I., Buser, N., Hafen, E. & Stocker, H. The WW domain protein kibra acts upstream of Hippo in *Drosophila*. *Dev. Cell* **18**, 309–316 (2010).

46. Yu, J. *et al.* Kibra functions as a tumor suppressor protein that regulates Hippo signaling in conjunction with Merlin and expanded. *Dev. Cell* **18**, 288–299 (2010).
47. Poon, C. L., Lin, J. I., Zhang, X. & Harvey, K. F. The Sterile 20-like Kinase Tao-1 controls tissue growth by regulating the Salvador–Warts–Hippo pathway. *Dev. Cell* **21**, 896–906 (2011).
48. Boggiano, J. C., Vanderzalm, P. J. & Fehon, R. G. Tao-1 phosphorylates Hippo/MST kinases to regulate the Hippo–Salvador–Warts tumor suppressor pathway. *Dev. Cell* **21**, 888–895 (2011).
49. Grzeschik, N. A., Parsons, L. M., Allott, M. L., Harvey, K. F. & Richardson, H. E. Lgl, aPKC, and Crumbs regulate the Salvador/Warts/Hippo pathway through two distinct mechanisms. *Curr. Biol.* **20**, 573–581 (2010).
50. Robinson, B. S., Huang, J., Hong, Y. & Moberg, K. H. Crumbs regulates Salvador/Warts/Hippo signaling in *Drosophila* via the FERM-domain protein expanded. *Curr. Biol.* **20**, 582–590 (2010).
51. Ling, C. *et al.* The apical transmembrane protein Crumbs functions as a tumor suppressor that regulates Hippo signaling by binding to expanded. *Proc. Natl Acad. Sci. USA* **107**, 10532–10537 (2010).
52. Chen, C. L. *et al.* The apical-basal cell polarity determinant Crumbs regulates Hippo signaling in *Drosophila*. *Proc. Natl Acad. Sci. USA* **107**, 15810–15815 (2010).
53. Tschop, K. *et al.* A kinase shRNA screen links LATS2 and the pRB tumor suppressor. *Genes Dev.* **25**, 814–830 (2011).
54. Baek, K. H. *et al.* Down's syndrome suppression of tumour growth and the role of the calcineurin inhibitor DSCR1. *Nature* **459**, 1126–1130 (2009).
55. Litovchick, L., Florens, L. A., Swanson, S. K., Washburn, M. P. & DeCaprio, J. A. DYRK1A protein kinase promotes quiescence and senescence through DREAM complex assembly. *Genes Dev.* **25**, 801–813 (2011).
56. Ionescu, A. *et al.* DYRK1A kinase inhibitors with emphasis on cancer. *Mini Rev. Med. Chem.* **12**, 1315–1329 (2012).
57. Malinge, S. *et al.* Increased dosage of the chromosome 21 ortholog Dyrk1a promotes megakaryoblastic leukemia in a murine model of Down syndrome. *J. Clin. Invest.* **122**, 948–962 (2012).
58. Gao, J. *et al.* Mirk/Dyrk1B mediates G0/G1 to S phase cell cycle progression and cell survival involving MAPK/ERK signaling in human cancer cells. *Cancer Cell Int.* **13**, 2 (2013).
59. Davis, S. J. *et al.* Functional analysis of genes in regions commonly amplified in high-grade serous and endometrioid ovarian cancer. *Clin. Cancer Res.* **19**, 1411–1421 (2013).
60. Fotaki, V. *et al.* Dyrk1A haploinsufficiency affects viability and causes developmental delay and abnormal brain morphology in mice. *Mol. Cell Biol.* **22**, 6636–6647 (2002).
61. Moller, R. S. *et al.* Truncation of the Down syndrome candidate gene DYRK1A in two unrelated patients with microcephaly. *Am. J. Hum. Gen.* **82**, 1165–1170 (2008).
62. van Bon, B. W. *et al.* Intragenic deletion in DYRK1A leads to mental retardation and primary microcephaly. *Clin. Genet.* **79**, 296–299 (2011).
63. Courcet, J. B. *et al.* The DYRK1A gene is a cause of syndromic intellectual disability with severe microcephaly and epilepsy. *J. Med. Genet.* **49**, 731–736 (2012).

METHODS

Drosophila melanogaster stocks. Riq knockdown was performed using two RNAi lines: *UAS-riqRi1* (KK 107076) from the Vienna *Drosophila* RNAi Center (VDRC) and *UAS-riqRi2* (14614R-1) from the Japanese National Institute of Genetics (NIG). Mnb knockdown was performed using two RNAi lines: *UAS-mnbRi1* (KK 107066) and *UAS-mnbRi2* (GD 28628) both from VDRC. The *riq* overexpression line was engineered by injection of a *pUAST-riq* construct cloned by PCR from the CG14614 complementary DNA obtained from DGRC (clone LD15927). Other stocks were: *mnb¹*, *ds^{UAO71}*, *dachs¹*, *dachs^{GCI3}*, *Dachs-GFP*, *UAS-mmb*, *UAS-ds*, *UAS-dsΔECD*, *UAS-ftΔICD*, *UAS-EYFP*, *ex-lacZ*, *ban-lacZ*, *th-lacZ*, *UAS-dachs*, *UAS-dachs* RNAi, *hh-Gal4*, *en-Gal4*, *m-Gal4*, *32B-Gal4* and *GMR-Gal4*. Clones of *UAS-riqRi1* and *UAS-mnbRi1* were obtained by crossing UAS lines with the *actin-Gal4* flip out stock: *hsflp; actin>CD2>Gal4*, *UAS-GFP*.

Measurement of wing size and leg length. Wing area from 20 female or male (as specified) flies reared at 25 °C was quantified using Adobe Photoshop. The tarsal segment (comprising T1 to 5) of the right back leg of 15 female adult flies was quantified using ImageJ.

Immunostaining. We used the following primary antibodies: mouse anti-β-galactosidase (#G4644, Sigma, 1:100), rat anti-Cubitus-interruptus (2A1, 1:50), mouse anti-Disc-large (4F3, 1:100), mouse anti-E-cadherin (7D6, 1:100) (all from Developmental Studies Hybridoma Bank), rabbit anti-DCAF7 (#NBP1-92589, Novus Biologicals, 1:100), rat anti-Dachs (gift from D. Strutt, 1:100), rat anti-Ds (gift from M. Simon, 1:1,000), rabbit-anti HA (#H6908, Sigma, 1:100) and mouse anti-V5 (#46-0705, Invitrogen, 1:100). Secondary antibodies (anti-rat, anti-mouse and anti-rabbit) were from Invitrogen (1:400). Third instar larval imaginal discs and pupal eye discs (44 h after puparium formation) were stained as in refs 64,65.

Statistics. Statistical tests used were as follows. Figures 1d and 2c and Supplementary Fig. S4f: 20 individual wings from 20 individual flies were analysed in one experiment. s.e.m. is represented and a one-way analysis of variance (ANOVA) test was used to assess statistical differences (for Figs 1d and 2c and Supplementary Fig. S4f, *** indicates $P < 0.001$, NS in Fig. 1d indicates 0.1001, and NS in Fig. 2c indicates $P > 0.9999$). Figures 1e and 2b: 15 individual legs from 15 individual flies were analysed in one experiment. s.e.m. is represented and a one-way ANOVA test was used to assess statistical significance (Fig. 1e *** indicates $P < 0.001$, ** in Fig. 2b indicates $P = 0.0015$). Figure 2c: 20 individual wings from 20 individual flies were analysed in one experiment. s.e.m. is represented and a *t*-test was used to assess statistical significance (** indicates $P < 0.001$). Figure 5i: 3 cell extracts from 3 independent experiments were analysed by western blotting and quantified using ImageJ. A one-way ANOVA test was used to assess statistical significance (** indicates a *P* value of 0.0019 and NS indicates a *P* value of 0.927). Supplementary Fig. S2: 4 cDNA preparations from 4 different tissue preparations of 30 wing discs each were subjected to quantitative real-time PCR. s.e.m. is represented and a *t*-test was used to assess statistical significance (** indicates a *P* value of 0.063). Statistics source data for Fig. 5i and Supplementary Fig. S2b can be found in Supplementary Table S1. In Figs 1b,c, 3a–i^o, 6a–i^o and Supplementary Figs S1a–e, S2a, S3a–g, S4a–e and S7a–b^o, qualitative observations were made on at least 10 samples (either wing discs, pupal eyes or adult eyes from different animals, or cultured S2 cells). Wing and leg images in Figs 1d–e and 2b–c^o and Supplementary Figs S3h and S4f,i are representative of specimens that were collected from either 20 animals (wings) or 15 animals (legs) and used for quantitative analyses. Western blots and kinase assays were repeated at least three times (Figs 1a, 2a, 4a–b^o, 5a–d and 5f–i and Supplementary Fig. S5a–f). In each experiment, no statistical method was used to predetermine sample size, the experiments were not randomized and the investigators were not blinded to allocation during experiments or outcome assessment.

Plasmids. The DsICD (DsΔECD) was amplified by PCR from pUAST–DsΔECD (ref. 40) and cloned into the pAc5.1 and GS-TAP vectors²⁸. The Riq open reading frame was PCR-amplified from DGRC clone LD15927, epitope-tagged (either V5 or Myc) and cloned into pAc5.1. pMT–Mnb.HA was obtained from I. Ederly⁶⁶. pMT–Mnb K386R.HA was generated by site-directed mutagenesis. pAc5.1–Wts.V5 and pAc5.1–Yki.HA were from D. Pan²⁷. pAc5.1–Hpo.FLAG and pAc5.1–Sav.myc were from N. Tapon⁶⁷. Portions of Wts were amplified by PCR and cloned into pAc5.1. pAc5.1–myc.HipK was described in ref. 33. Wts1 was cloned into pGEX–4T1 for bacterial expression. pGEX–CACYBP was from C. House.

Cell culture, transfection and western blot analysis. S2 cells from the *Drosophila* Genomics Resource Center were cultured in Schneider's *Drosophila*

medium (Gibco) supplemented with 10% FBS (Gibco) and 1% penicillin/streptomycin (Gibco). Cells were transfected with the indicated plasmids using the Effectene transfection reagent (Qiagen). CuSO₄ was added to culture media at a final concentration of 0.35 mM when using pMT-based plasmids. In some instances, cells were treated with 50 μg dsRNA specific for Mnb or Riq for 48 h. After 48 h, cells were lysed using RIPA buffer consisting of 10 mM NaP_i buffer, at pH 7.8, 60 mM NaCl, 1% Triton X-100, 0.5% deoxycholic acid, 0.1% SDS, 10% glycerol, 25 mM β-glycerol phosphate, 50 mM sodium fluoride, 2 mM sodium pyrophosphate, 1 mM sodium orthovanadate, and protease inhibitor (Complete, Roche), subjected to SDS–PAGE then transferred to PVDF membrane (Millipore). In some instances, lysates were treated with calf intestinal phosphatase (Sigma) at 37 °C for 2 h before SDS–PAGE. To visualize differences in Wts mobility, 3–8% Tris acetate gels were used (Invitrogen). For other experiments, 4–12% Bis-Tris gels were used. Membranes were immunoblotted with the following antibodies: rabbit anti-HA (#H6908, Sigma), mouse anti-V5, mouse anti-Tubulin (#46-0705 and #32-2600 from Invitrogen) and rabbit anti-phospho-S168-Yki (gift from N. Tapon). HRP-coupled secondary antibodies were from Dako. Detection was performed using the ECL prime Western Blotting Detection reagent from Amersham. Images were taken using the ChemiDoc MP (Biorad). Quantification of bands was performed with ImageJ.

Kinase assays. S2 cells were transfected with Mnb or Mnb K386R. Two days after transfection, cells were lysed in DISC lysis buffer (150 mM NaCl, 2 mM EDTA, 1% Triton X-100, 10% glycerol, 20 mM Tris at pH 7.5, 10 mM NaF, 2 mM Na pyrophosphate, 5 mM β-glycerophosphate and PhosStop phosphatase inhibitor cocktail (Roche) and Complete Mini protease inhibitor cocktail (Roche)) and immunoprecipitated using rabbit anti-HA (#H6908, Sigma). BL-21 bacteria transformed with pGEX–4T1–GST–Wts1 or pGEX–CACYBP were incubated with 1 mM IPTG at 37 °C to induce protein expression. Recombinant proteins were purified using glutathione Sepharose and eluted in 50 mM Tris–HCl, 10 mM glutathione and 0.05% Triton X-100, at pH 8. Equivalent amounts of GST–Wts1 and pGEX–CACYBP were used in each kinase assay. Equivalent amounts of immunoprecipitates were divided into the combinations noted in the figure legend in kinase buffer (50 mM HEPES at pH 7.4, 10 mM MgCl₂, 1 mM dithiothreitol, 10% glycerol, 1 mM EDTA, 1 mM EGTA, 100 mM NaCl, 1 mM NaF, 5 mM β-glycerophosphate, 100 μM ATP, PhosStop phosphatase inhibitor cocktail and Complete Mini protease inhibitor cocktail). As in ref. 68, 5 μCi[γ-³²P]ATP (Perkin Elmer) was added to each sample and incubated at 30 °C for 30 min. The reaction was stopped by the addition of 5× protein loading buffer, boiled at 95 °C and subjected to SDS–PAGE. Gels were dried and exposed to a Phosphorimager screen (Molecular Dynamic) and analysed using the Typhoon Trio Phosphorimager and ImageQuant software (GE Healthcare) as in ref. 47.

Mass spectrometry. Independent *in vitro* kinase assays performed as above with cold ATP were digested overnight in trypsin, and then analysed by mass spectrometry at either the Bio21 Mass Spectrometry Facility (University of Melbourne) or the Taplin Mass Spectrometry Facility (Harvard University).

Quantitative real-time PCR. RNA was extracted from wing imaginal discs by Trizol (Invitrogen), and used to generate cDNA with Superscript III (Invitrogen). Quantitative PCR reactions were performed on Applied Biosystems Step One Plus software with Fast SYBR Green Master Mix (Applied Biosystems) and primers designed to detect *riq* and *Actin 5C* messenger RNA as in ref. 69.

64. Milton, C. C., Zhang, X., Albanese, N. O. & Harvey, K. F. Differential requirement of Salvador–Warts–Hippo pathway members for organ size control in *Drosophila melanogaster*. *Development* **137**, 735–743 (2010).
65. Harvey, K. F., Pfeleger, C. M. & Hariharan, I. K. The *Drosophila* Mst ortholog, hippo, restricts growth and cell proliferation and promotes apoptosis. *Cell* **114**, 457–467 (2003).
66. Chiu, J. C., Ko, H. W. & Ederly, I. NEMO/NLK phosphorylates PERIOD to initiate a time-delay phosphorylation circuit that sets circadian clock speed. *Cell* **145**, 357–370 (2011).
67. Pantalacci, S., Tapon, N. & Leopold, P. The Salvador partner Hippo promotes apoptosis and cell-cycle exit in *Drosophila*. *Nat. Cell Biol.* **5**, 921–927 (2003).
68. Callus, B. A., Verhagen, A. M. & Vaux, D. L. Association of mammalian sterile twenty kinases, Mst1 and Mst2, with hSalvador via C-terminal coiled-coil domains, leads to its stabilization and phosphorylation. *FEBS J.* **273**, 4264–4276 (2006).
69. Harvey, K. F. *et al.* FOXO-regulated transcription restricts overgrowth of Tsc mutant organs. *J. Cell Biol.* **180**, 691–696 (2008).

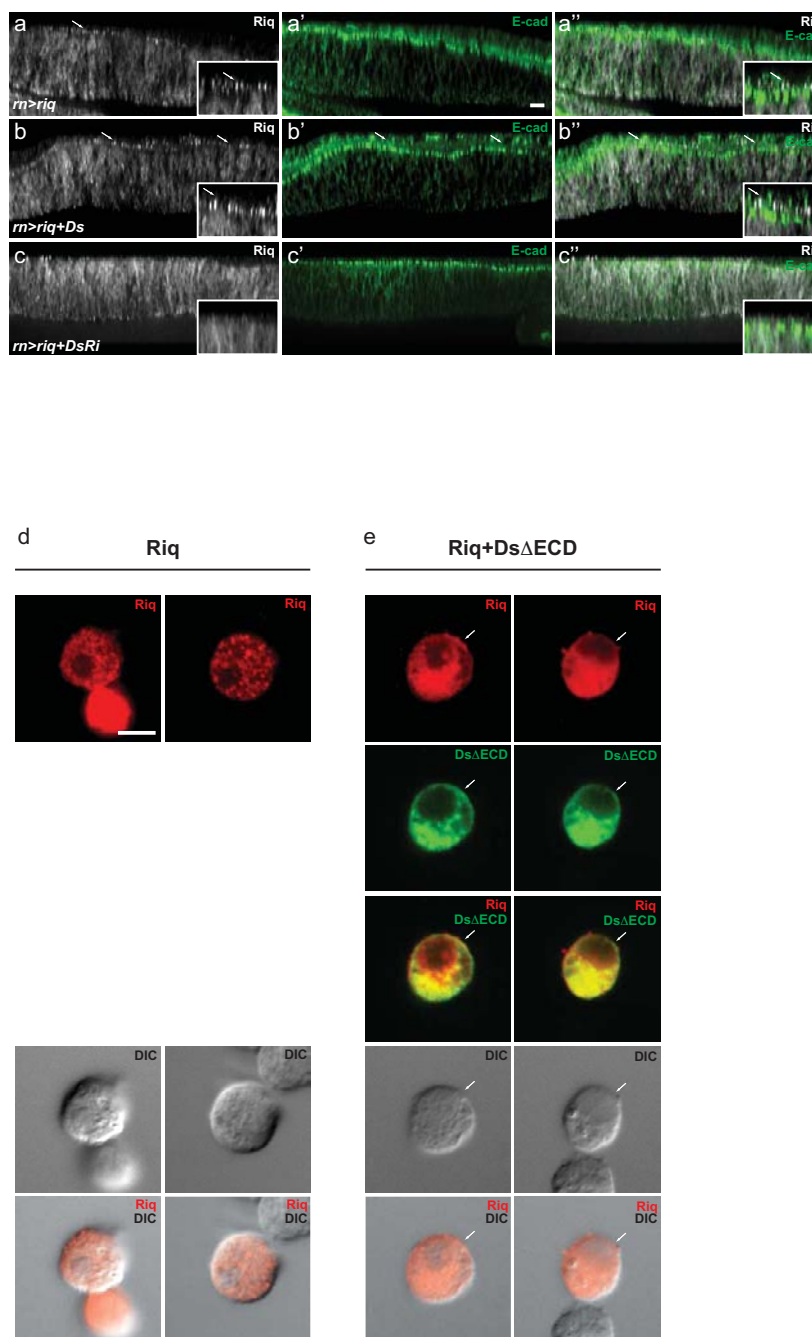


Figure S1 Dachshous promotes localization of Riquiqui to apical junctions and cell membranes. (a-c'') X-Z cross-sections of *D. melanogaster* third instar larval wing imaginal discs expressing the following elements: (a, a', a'') *m-Gal4*, *UAS-riq*; (b, b', b'') *m-Gal4*, *UAS-riq* and *UAS-ds*; (c, c', c'') *m-Gal4*, *UAS-riq* and *UAS-dsRi*. Riq is in white, E-cadherin marks the adherens junction in green. Arrows indicate Riq protein that is present at apical junctions in Ds-expressing tissues. Magnified images are inset in

(a) (a') (b) and (b'). Merged images are on the right. Riq was junctionally localised immediately apical to E cadherin. Riq was largely absent from apical junctions of tissues where Ds was depleted by RNAi. (d and e) *D. melanogaster* S2 cells expressing either Riq (d) or Riq and DsΔECD (e). Riq is in red, DsΔECD is green, Direct interference contrast (DIC) images are grey. Arrows indicate Riq protein that is present at cell membranes in DsΔECD-expressing cells. Scale bar represents 10μm in (a-c'') and 5μm in (d) and (e).

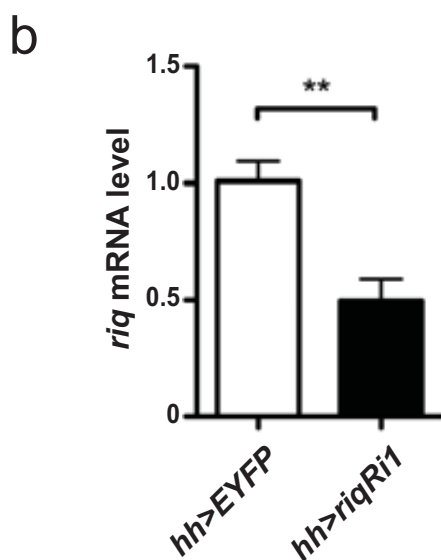
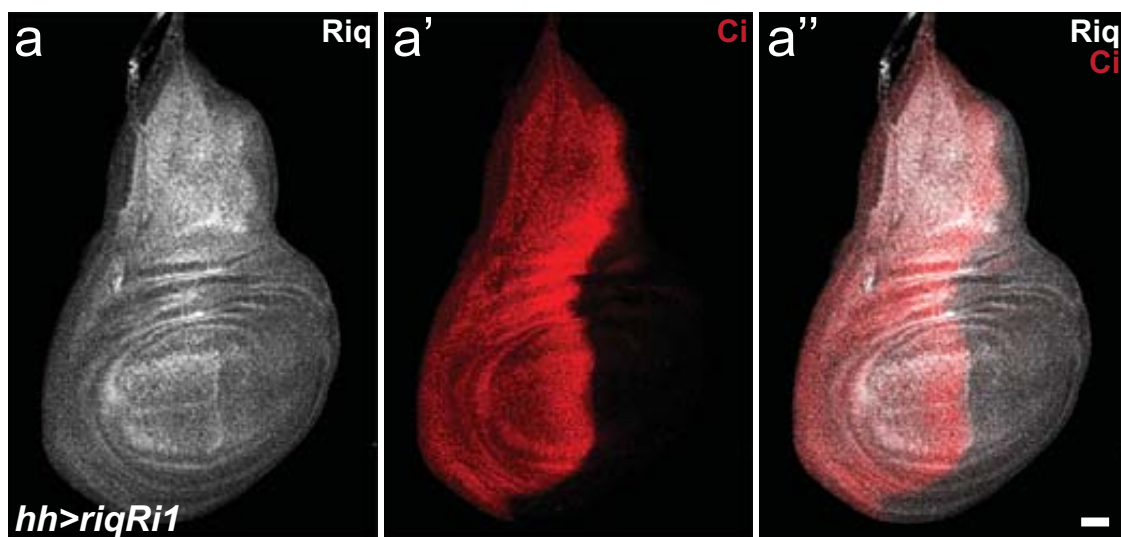


Figure S2 *UAS-riq RNAi* transgenes decrease Riq expression. (a) A wing imaginal disc from a third instar *D. melanogaster* larva expressing *UAS-riq1* under the control of *hh-Gal4*. Riq expression (grey in a) was assessed using an antibody directed against DCAF7 (human homologue of Riq). Cubitus interruptus (Ci) expression (red in a') marked the anterior compartment of wing imaginal discs. A merged image is

shown in (a''). (b) The level of *riq* mRNA relative to the control *actin5C* mRNA, assessed by QRT-PCR, in wing imaginal discs harbouring the following transgenes: *hh-Gal4* and *UAS-EYFP*; or *hh-Gal4* and *UAS-riq1*. Data is presented as mean ± SEM, n=3, ** = p<0.01. Scale bar represents 50µm in (a). Statistics source data for Fig. S2b is available in Supplementary Table S1.

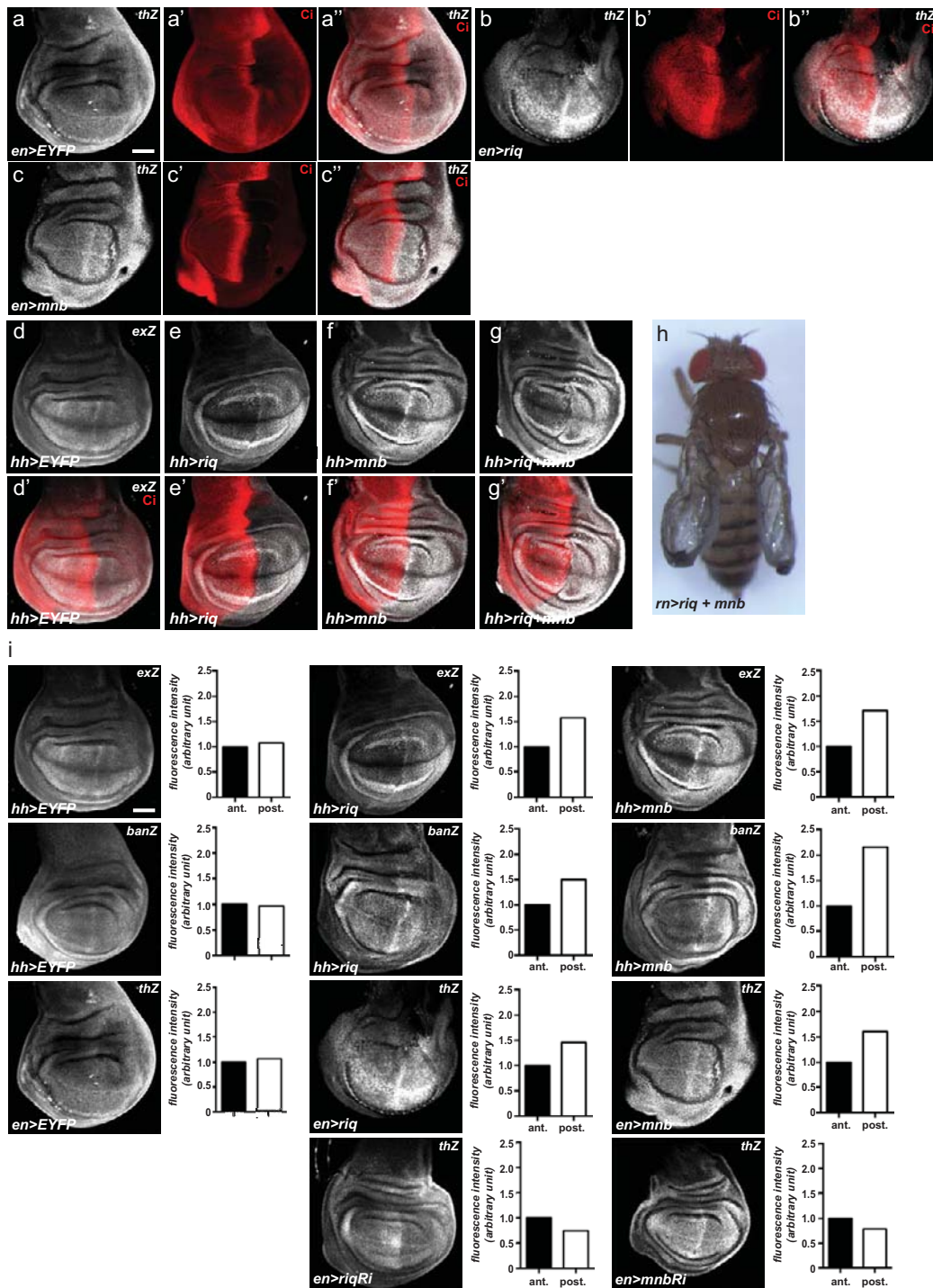


Figure S3 Riquiqui and Minibrain regulate SWH pathway activity. Wing imaginal discs from third instar *D. melanogaster* larvae harbouring the following elements: (a-a'') *en-Gal4, UAS-EYFP* and *th-lacZ*; (b-b'') *en-Gal4, UAS-riq* and *th-lacZ*; (c-c'') *en-Gal4, UAS-mnb* and *th-lacZ*; (d, d') *hh-Gal4, UAS-EYFP* and *ex-lacZ*; (e, e') *hh-Gal4, UAS-riq* and *ex-lacZ*; (f, f') *hh-Gal4, UAS-mnb* and *ex-lacZ*; (g, g') *hh-Gal4, UAS-riq, UAS-mnb* and *ex-lacZ*. Yki activity (grey) was reported by *th-lacZ* (a-c) or *ex-lacZ* (d-g). All transgenes were expressed in the posterior compartment of wing imaginal discs; Ci expression (red) marks the anterior compartment. Merged images are shown in (a''-c'' and in d'-g'). (h)

An adult female fly expressing both *riq* and *mnb* under control of the *rn-Gal4* driver. Unlike driving expression of *riq* and *mnb* alone, driving expression of both transgenes together caused severe folding and crumpling of wings, which prevented quantification of their size. (e) Quantification of LacZ expression driven by *ex-lacZ*, *ban-lacZ* or *th-lacZ* in wing imaginal discs displayed in Fig. 3 and Supplementary Fig. S3a-c. Anterior is to the left. For each disc fluorescence intensity was measured by ImageJ in two boxes of defined size in both the anterior (ant.) and posterior (post.) compartments. These values were averaged and plotted for each experiment. Scale bar represents 50µm.

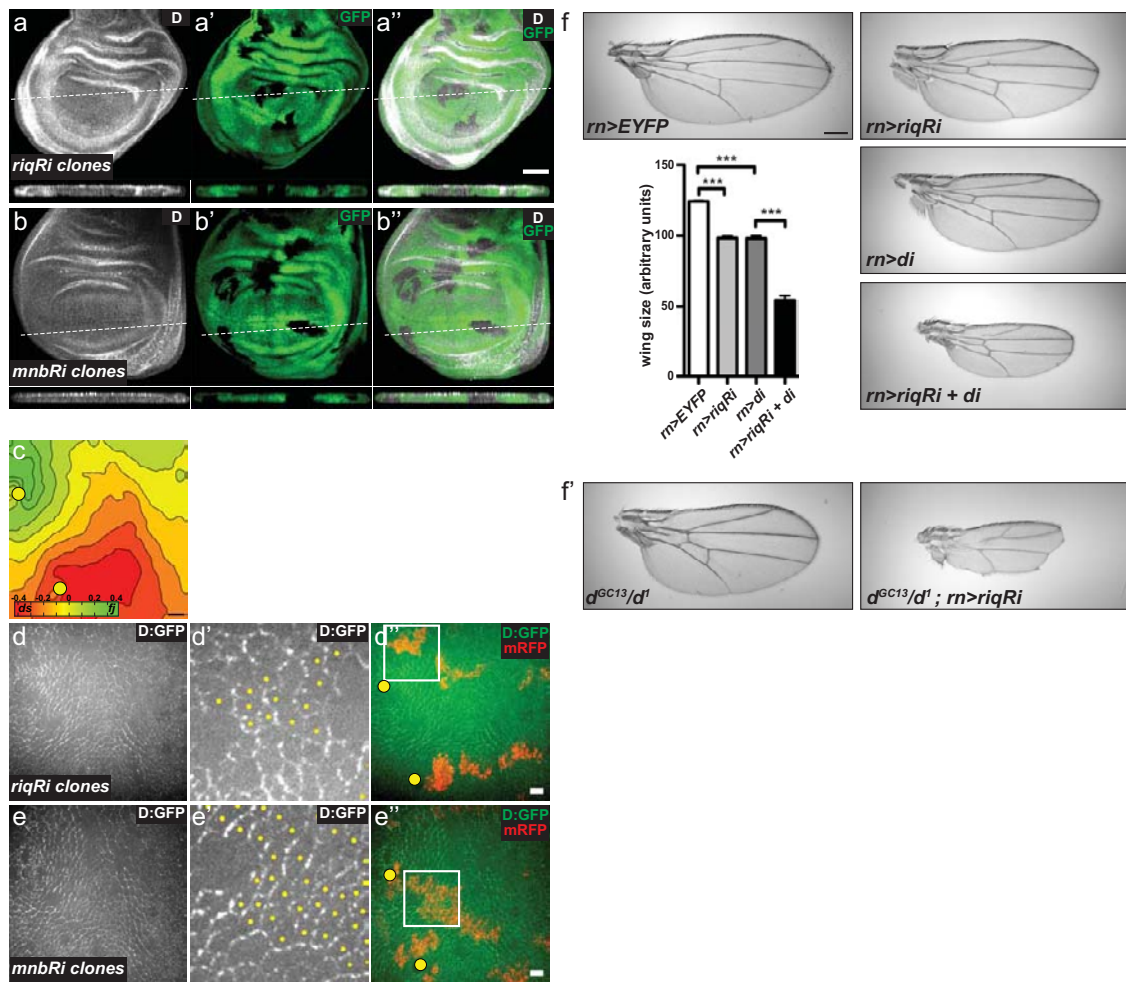


Figure S4 Riquiqui and Minibrain affect wing growth independently of Dachs. Wing imaginal discs from third instar *D. melanogaster* larvae containing clones of *UAS-riq1* (a) or *UAS-mnb1* (b) were stained for Dachs (grey in a and b). Clones were positively marked by co-expression of GFP (a' and b'). Merged images are shown in (a'' and b''). X-Z sections through the wing pouch are shown below planar sections of wing discs in a-b''. Dashed lines represent the section used to obtain X-Z images. No changes in Dachs expression or localization were observed. (d-e'') All images were recorded in pupal scutellum tissue (right-sided hemi-scutellum) at 20 hour after pupa formation. Anterior is to the right, the midline is to the top. Yellow circles mark the macrocheatae. Spatial information on the Fj-Ds gradient is shown in c as in¹. Flip out clones

of *UAS-riq1* and *UAS-mnb1* were generated and marked in red (d'') and (e'') respectively). White boxes are magnified in d' and e'. Yellow dots mark the mutant cells abutting wt cells (d' and e'). In these Flip-Out clones no clear reduction of D:GFP levels was observed when compared with the surrounding tissue. There is also no clear repolarization of D:GFP near clone boundaries. (f) Wing area from adult female flies expressing *UAS-EYFP* as control, *UAS-riq1*, *UAS-dachs RNAi (di)*, *UAS-riq1* concomitantly with *UAS-di*, under the control of *rn-Gal4* (n=20 for each genotype). Representative images of each genotype are shown. Data is presented as mean ± SEM, *** = p<0.001. These results suggest Dachs and Riq control tissue growth by acting in parallel. Scale bars represents 50µm in (a) and (b), 10µm in (c), (d) and (e), and 200µm in (f).

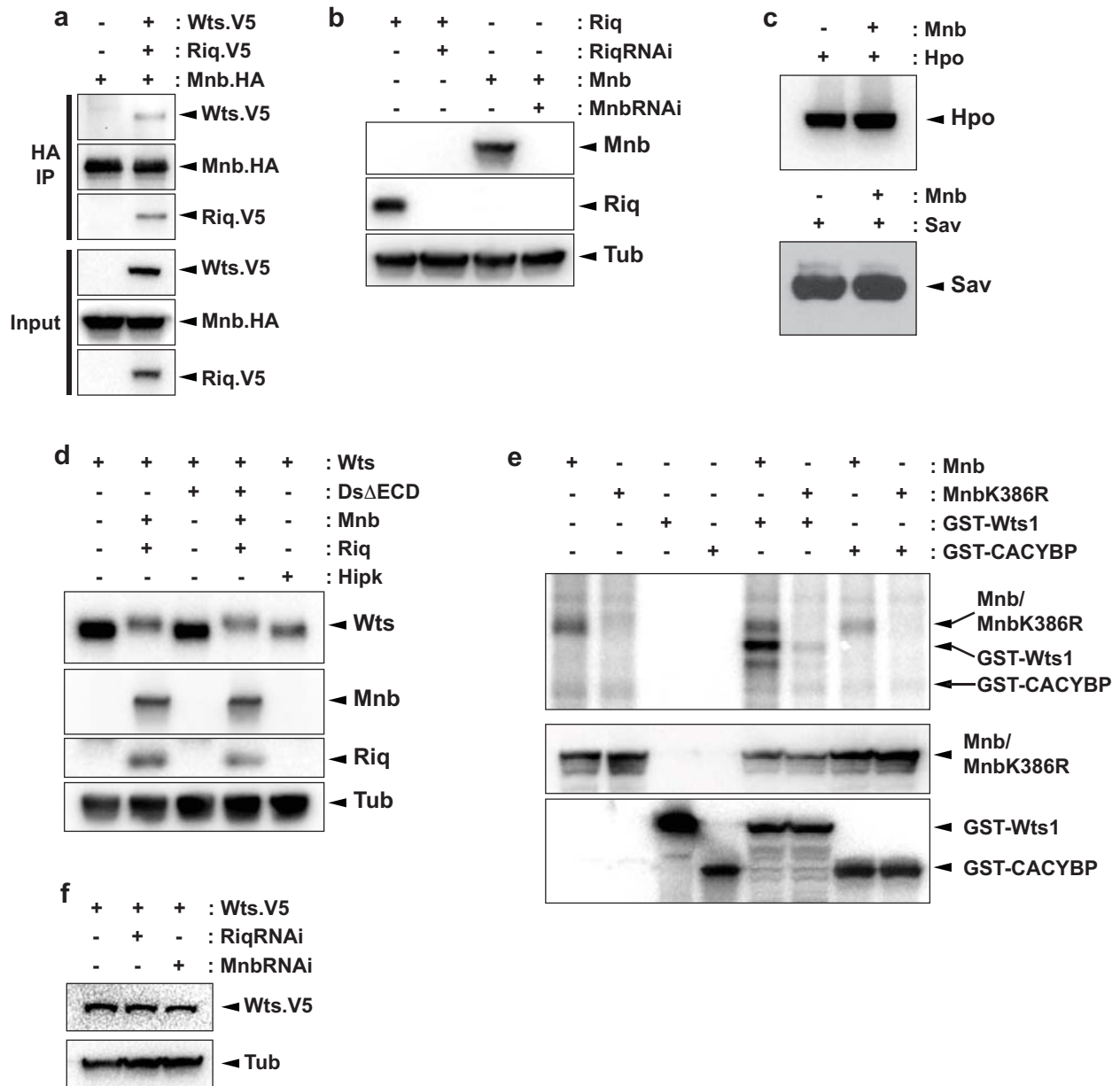


Figure S5 Riquiqui, Minibrain and Warts physically interact with each other and Minibrain phosphorylates Warts. (a) S2 cells were transfected with the indicated plasmids and immunoprecipitations performed using anti-HA antibodies. Subsequently, immunoprecipitates and input lysates were subjected to SDS-PAGE and Western blotted to reveal the indicated proteins. (b-d) Western blot analysis of lysates from S2 cells transfected with the indicated plasmids and Western blotted to reveal the indicated proteins. In (b) Riq or Mnb were expressed in S2 cells in the presence or absence of dsRNA specific for Riq or Mnb, respectively. In (c) Mnb did not induce changes in Hpo or Sav mobility. In (d) Mnb, but not Hipk influenced Wts mobility. (e)

Kinase assays performed using recombinant GST-Wts1 or GST-CACYBP as substrates and either Mnb or Mnb K386R immunoprecipitated from S2 cells. Immunopurified and recombinant proteins were incubated alone or together in kinase buffer containing γ^{32} P-ATP and subjected to SDS-PAGE (upper panel). Western blotting was used to detect input proteins (lower panels). Mnb phosphorylated GST-Wts1 but not the negative control substrate GST-CACYBP. (f) V5-tagged Wts was expressed in the presence or absence of dsRNA specific for Riq or Mnb in S2 cells. Cells were lysed and lysates were immunoblotted using antibodies to V5 and to Tubulin as a loading control. Wts levels were unchanged when Riq or Mnb were depleted from cells by RNAi.

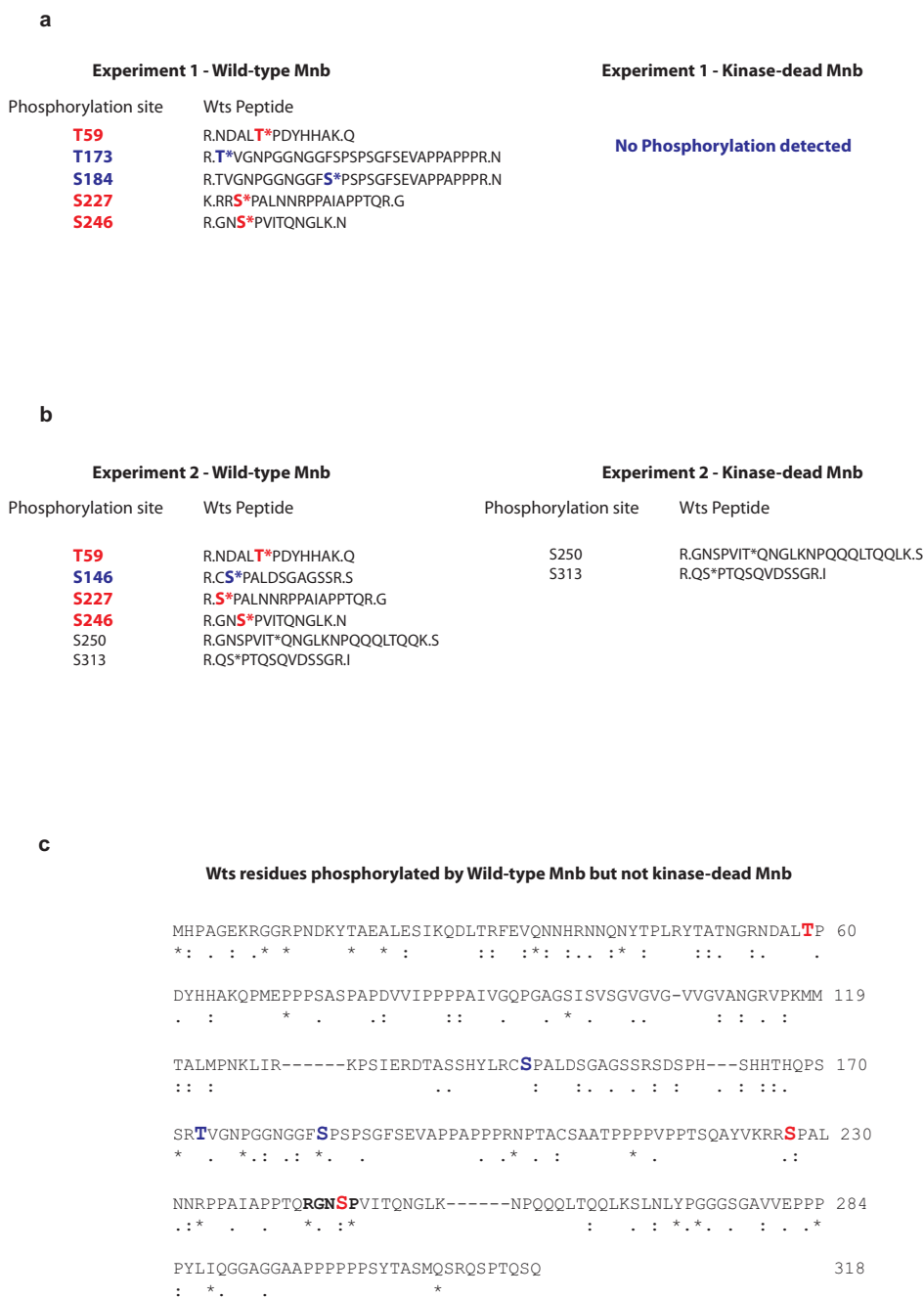


Figure S6 Minibrain phosphorylates six amino acids in the Warts protein, including a DYRK1A consensus site. (a and b) Wts1 (amino acids 1-318 of Wts) peptides that possessed amino acids that were phosphorylated when incubated with either wild-type Mnb or kinase-dead Mnb (Mnb-KD) immunoprecipitates. Experiments 1 and 2 were performed independently and analyzed by different mass spectrometry facilities. In experiment 1, five Wts amino acids were phosphorylated by wild-type Mnb with high confidence, whereas Mnb-KD induced no observable phosphorylation. In experiment 2, six Wts amino acids were phosphorylated by wild-type Mnb with high confidence, whilst two amino acids were phosphorylated in the presence of Mnb-KD. Amino acids that were phosphorylated by Mnb, but not Mnb-KD, are highlighted; amino acids that were phosphorylated in both

independent experiments are red and amino acids that were phosphorylated in only one experiment are blue. (c) A summary of mass spectrometry data outlined in (a) and (b). The amino acid sequence of Wts1 is shown and the degree of conservation with human LATS1, as assessed by CLUSTAL, is indicated below: * indicates perfect conservation, : indicates strongly similar; . indicates weakly similar. As in (a) and (b), amino acids that were phosphorylated in both independent experiments by Mnb, but not Mnb-KD, are highlighted in red and amino acids that were phosphorylated by Mnb in only one experiment are in blue. The Wts sequence that was phosphorylated by Mnb and closely resembles a DYRK1A consensus site (RPXS/TP)² is in bold font. Of note, this site was phosphorylated in each experiment and is conserved between Wts and LATS1.

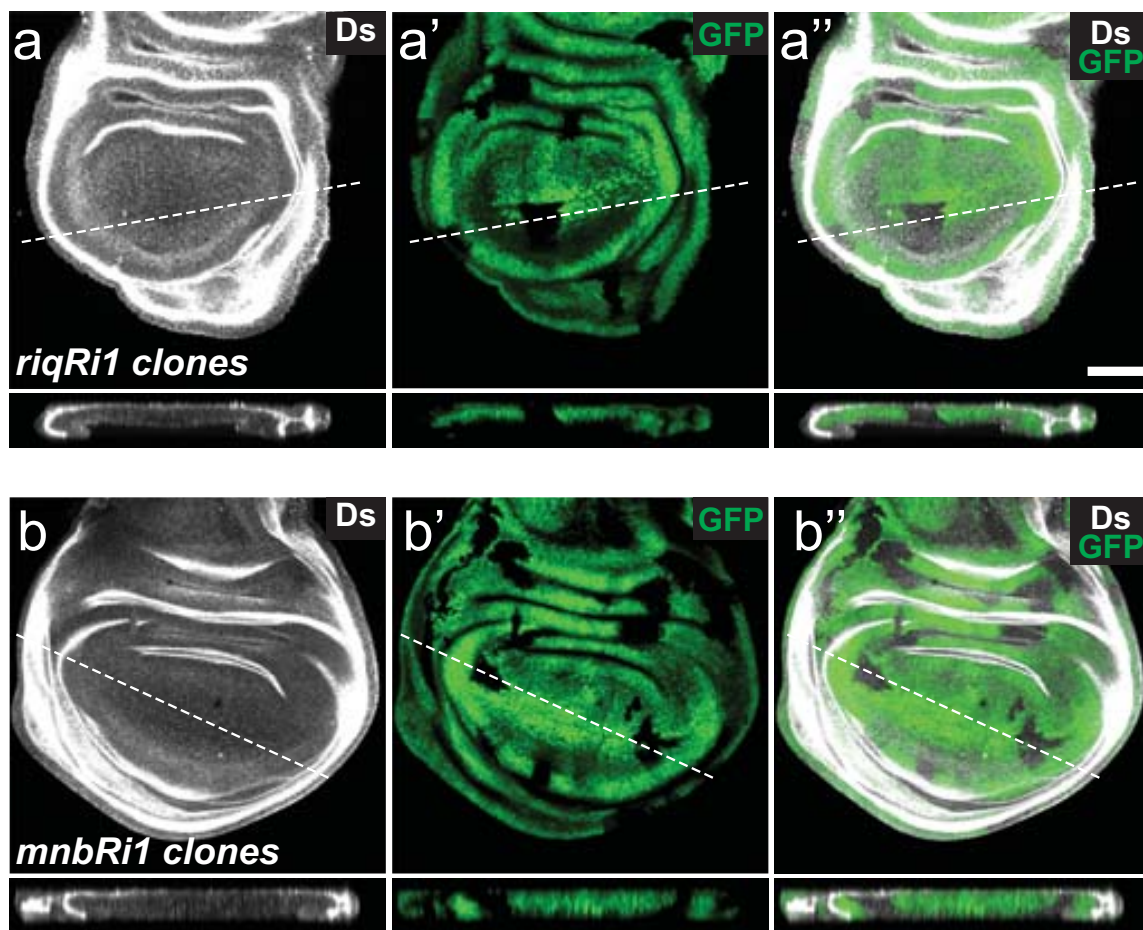


Figure S7 Reduction of Riq or Mnb expression does not affect Dachsous expression. Wing imaginal discs from third instar *D. melanogaster* larvae containing clones of *UAS-riq1* (a) or *UAS-mnb1* (b) were stained for Ds (grey in a and b). Clones were positively marked by co-expression of GFP (a'

and b'). Merged images are shown in (a'' and b''). X-Z sections through the wing pouch are shown below planar sections of wing discs in a-b''. Dashed lines represent the section used to obtain X-Z images. Scale bar represents 50µm.

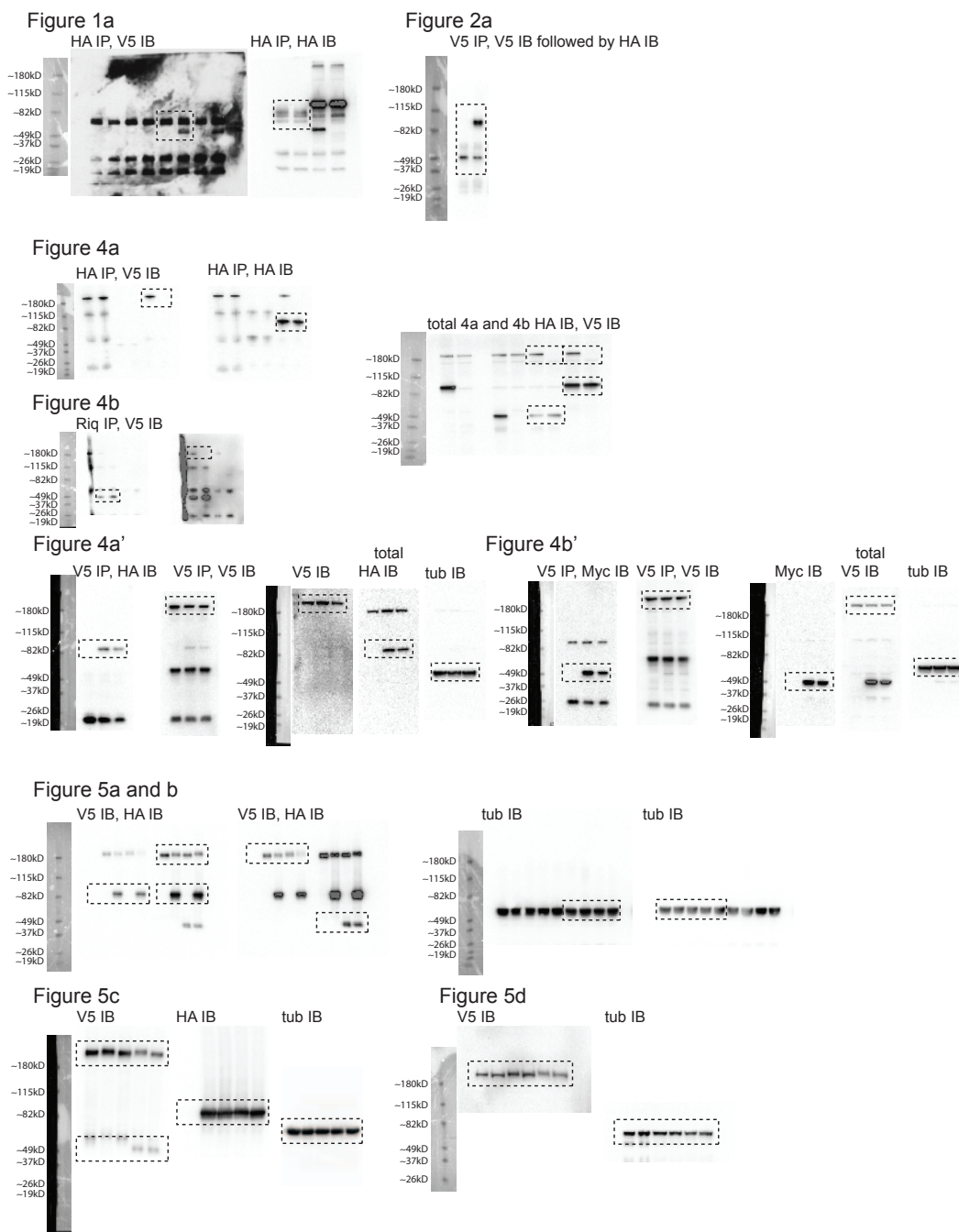
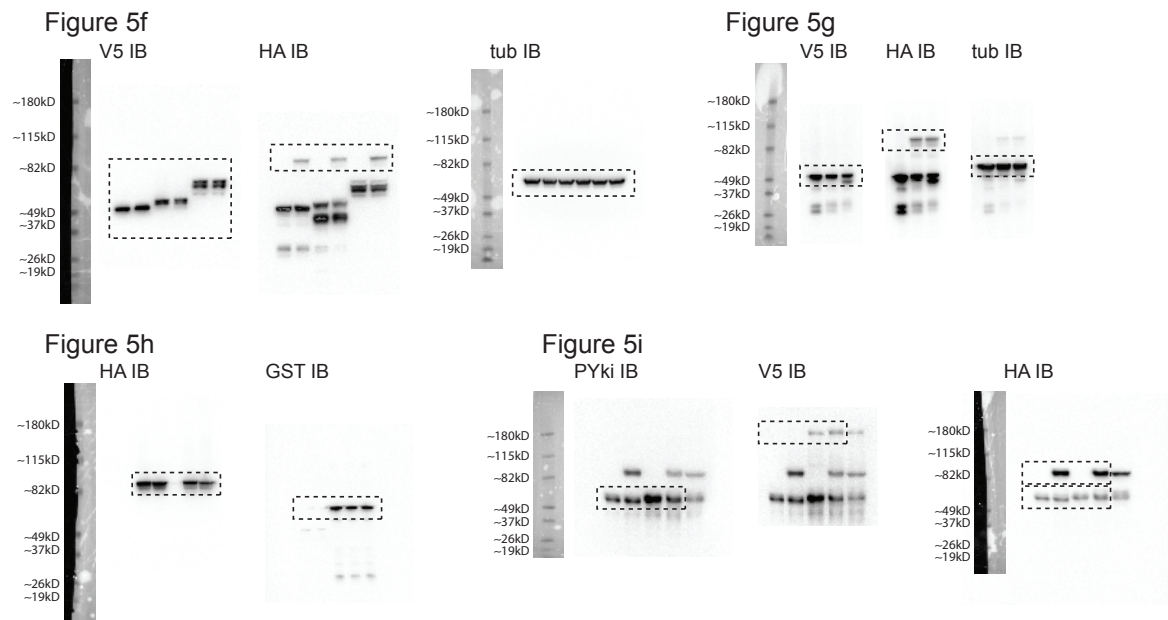


Figure S8 Full scan



Supplementary References

1. Bosveld, F. *et al.* Mechanical control of morphogenesis by Fat/Dachsous/Four-jointed planar cell polarity pathway. *Science* **336**, 724-727 (2012).
2. Himpel, S. *et al.* Specificity determinants of substrate recognition by the protein kinase DYRK1A. *J Biol Chem* **275**, 2431-2438 (2000).

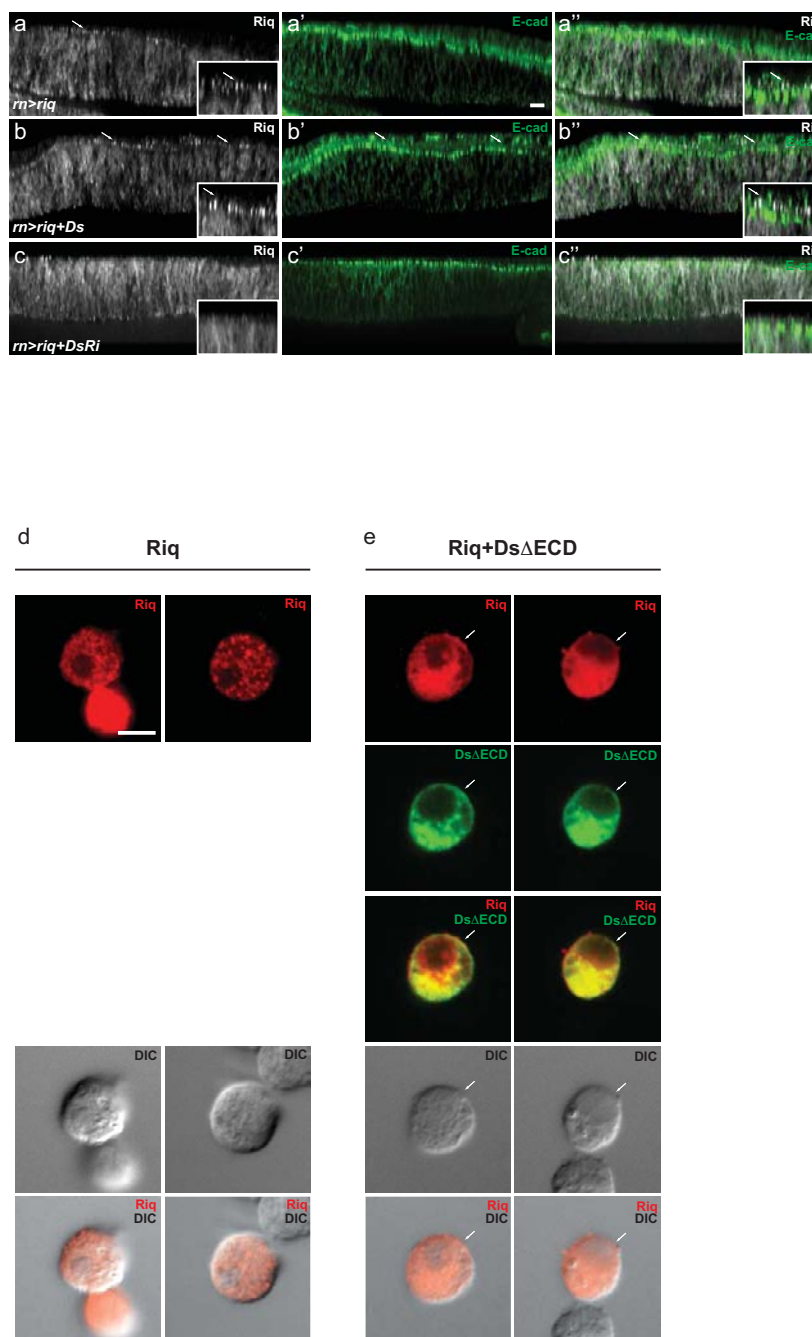


Figure S1 Dachshous promotes localization of Riquiqui to apical junctions and cell membranes. (a-c") X-Z cross-sections of *D. melanogaster* third instar larval wing imaginal discs expressing the following elements: (a, a', a") *rn-Gal4*, *UAS-riq*; (b, b', b") *rn-Gal4*, *UAS-riq* and *UAS-ds*; (c, c', c") *rn-Gal4*, *UAS-riq* and *UAS-dsRi*. Riq is in white, E-cadherin marks the adherens junction in green. Arrows indicate Riq protein that is present at apical junctions in Ds-expressing tissues. Magnified images are inset in

(a) (a') (b) and (b'). Merged images are on the right. Riq was junctionally localised immediately apical to E cadherin. Riq was largely absent from apical junctions of tissues where Ds was depleted by RNAi. (d and e) *D. melanogaster* S2 cells expressing either Riq (d) or Riq and DsΔECD (e). Riq is in red, DsΔECD is green, Direct interference contrast (DIC) images are grey. Arrows indicate Riq protein that is present at cell membranes in DsΔECD-expressing cells. Scale bar represents 10μm in (a-c") and 5μm in (d) and (e).

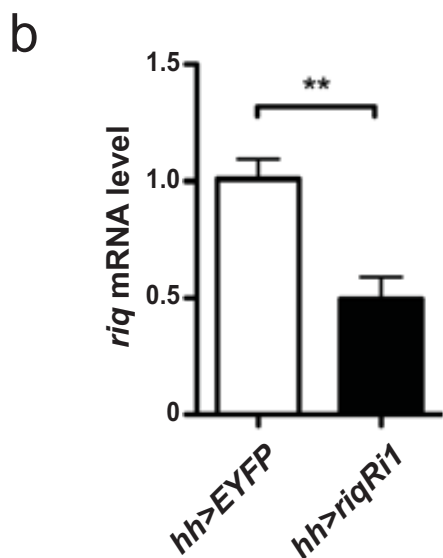
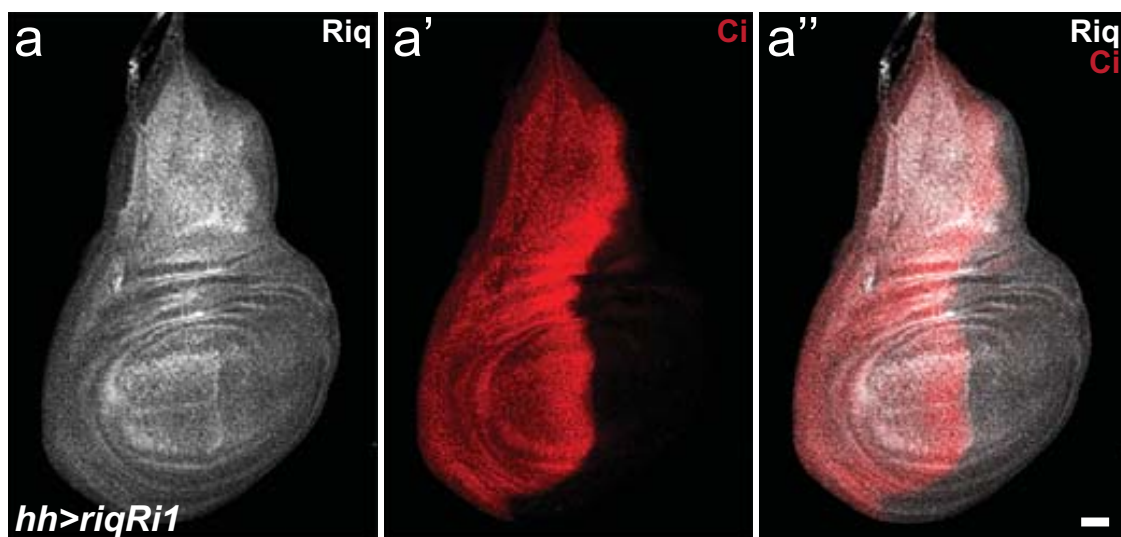


Figure S2 *UAS-riq RNAi* transgenes decrease Riq expression. (a) A wing imaginal disc from a third instar *D. melanogaster* larva expressing *UAS-riq1* under the control of *hh-Gal4*. Riq expression (grey in a) was assessed using an antibody directed against DCAF7 (human homologue of Riq). Cubitus interruptus (Ci) expression (red in a') marked the anterior compartment of wing imaginal discs. A merged image is

shown in (a''). (b) The level of *riq* mRNA relative to the control *actin5C* mRNA, assessed by QRT-PCR, in wing imaginal discs harbouring the following transgenes: *hh-Gal4* and *UAS-EYFP*; or *hh-Gal4* and *UAS-riq1*. Data is presented as mean ± SEM, n=3, ** = p<0.01. Scale bar represents 50µm in (a). Statistics source data for Fig. S2b is available in Supplementary Table S1.

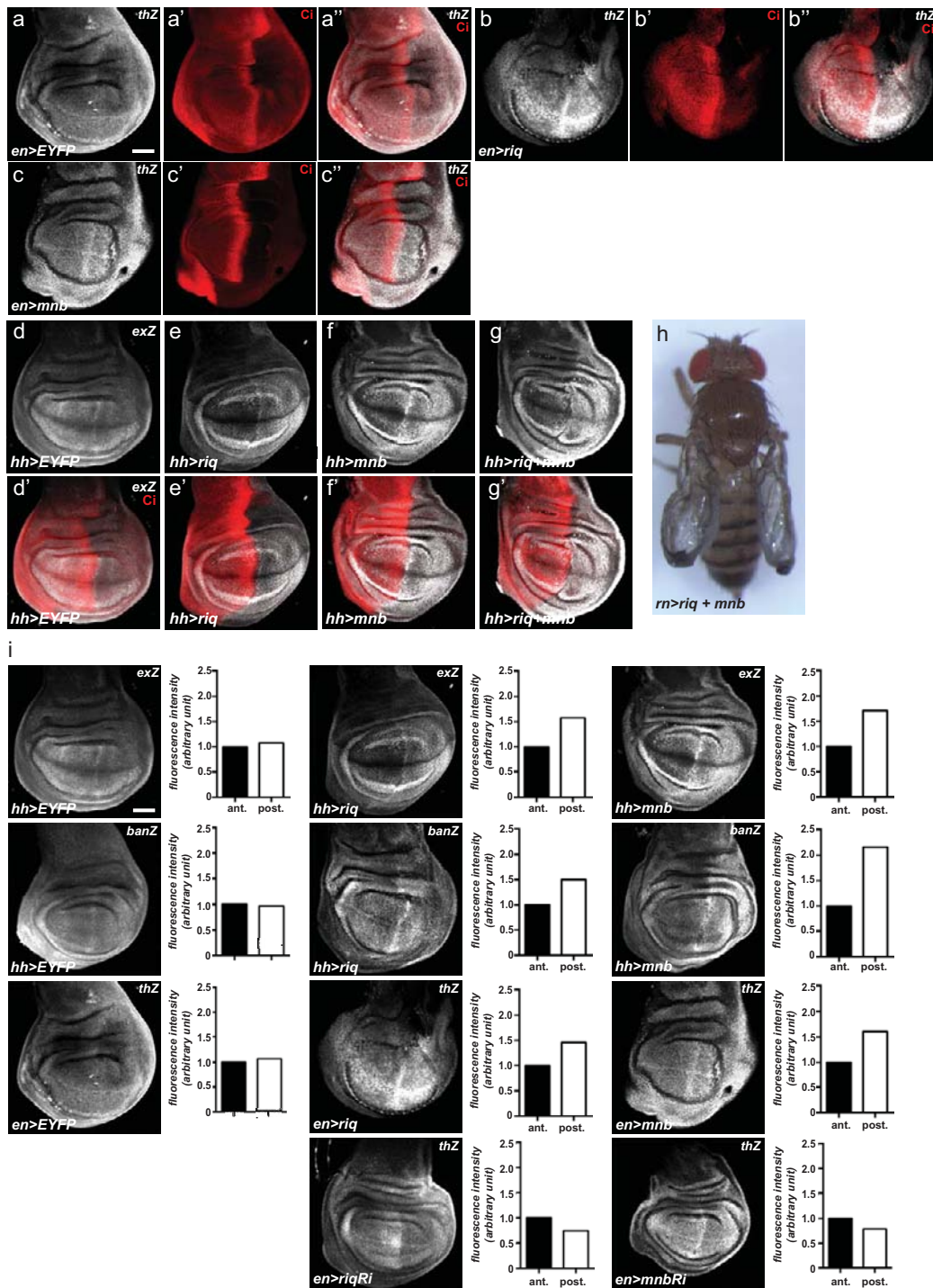


Figure S3 Riquiqui and Minibrain regulate SWH pathway activity. Wing imaginal discs from third instar *D. melanogaster* larvae harbouring the following elements: (a-a'') *en-Gal4*, *UAS-EYFP* and *th-lacZ*; (b-b'') *en-Gal4*, *UAS-riq* and *th-lacZ*; (c-c'') *en-Gal4*, *UAS-mnb* and *th-lacZ*; (d, d') *hh-Gal4*, *UAS-EYFP* and *ex-lacZ*; (e, e') *hh-Gal4*, *UAS-riq* and *ex-lacZ*; (f, f') *hh-Gal4*, *UAS-mnb* and *ex-lacZ*; (g, g') *hh-Gal4*, *UAS-riq*, *UAS-mnb* and *ex-lacZ*. Yki activity (grey) was reported by *th-lacZ* (a-c) or *ex-lacZ* (d-g'). All transgenes were expressed in the posterior compartment of wing imaginal discs; Ci expression (red) marks the anterior compartment. Merged images are shown in (a''-c'' and in d'-g'). (h)

An adult female fly expressing both *riq* and *mnb* under control of the *rn-Gal4* driver. Unlike driving expression of *riq* and *mnb* alone, driving expression of both transgenes together caused severe folding and crumpling of wings, which prevented quantification of their size. (e) Quantification of LacZ expression driven by *ex-lacZ*, *ban-lacZ* or *th-lacZ* in wing imaginal discs displayed in Fig. 3 and Supplementary Fig. S3a-c. Anterior is to the left. For each disc fluorescence intensity was measured by ImageJ in two boxes of defined size in both the anterior (ant.) and posterior (post.) compartments. These values were averaged and plotted for each experiment. Scale bar represents 50 μm.

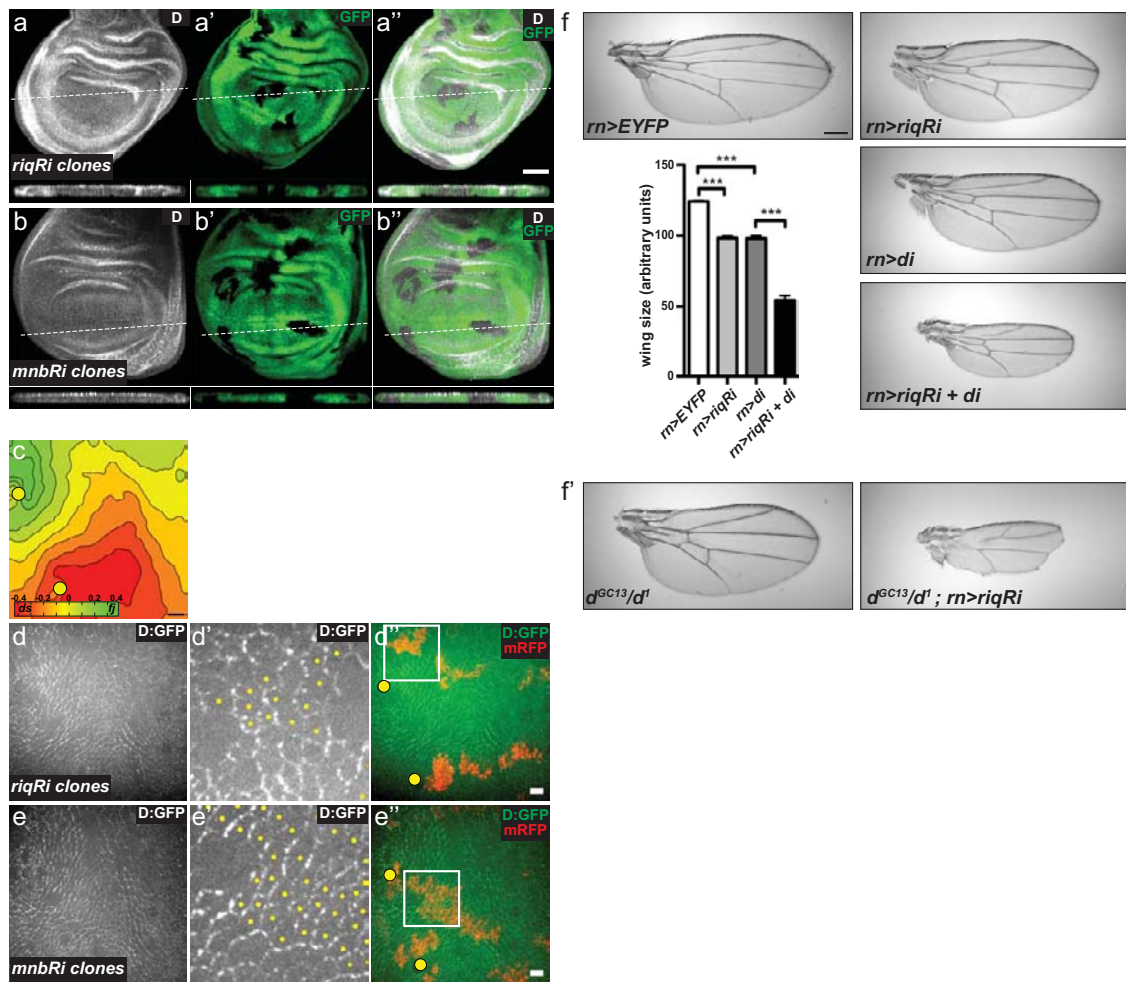


Figure S4 Riquiqui and Minibrain affect wing growth independently of Dachs. Wing imaginal discs from third instar *D. melanogaster* larvae containing clones of *UAS-riq1* (a) or *UAS-mnb1* (b) were stained for Dachs (grey in a and b). Clones were positively marked by co-expression of GFP (a' and b'). Merged images are shown in (a'' and b''). X-Z sections through the wing pouch are shown below planar sections of wing discs in a-b''. Dashed lines represent the section used to obtain X-Z images. No changes in Dachs expression or localization were observed. (d-e'') All images were recorded in pupal scutellum tissue (right-sided hemi-scutellum) at 20 hour after pupa formation. Anterior is to the right, the midline is to the top. Yellow circles mark the macrocheatae. Spatial information on the Fj-Ds gradient is shown in c as in¹. Flip out clones

of *UAS-riq1* and *UAS-mnb1* were generated and marked in red (d'' and e'' respectively). White boxes are magnified in d' and e'. Yellow dots mark the mutant cells abutting wt cells (d' and e'). In these Flip-Out clones no clear reduction of D:GFP levels was observed when compared with the surrounding tissue. There is also no clear repolarization of D:GFP near clone boundaries. (f) Wing area from adult female flies expressing *UAS-EYFP* as control, *UAS-riq1*, *UAS-dachs RNAi (di)*, *UAS-riq1* concomitantly with *UAS-di*, under the control of *rn-Gal4* (n=20 for each genotype). Representative images of each genotype are shown. Data is presented as mean ± SEM, *** = p<0.001. These results suggest Dachs and Riq control tissue growth by acting in parallel. Scale bars represents 50µm in (a) and (b), 10µm in (c), (d) and (e), and 200µm in (f).

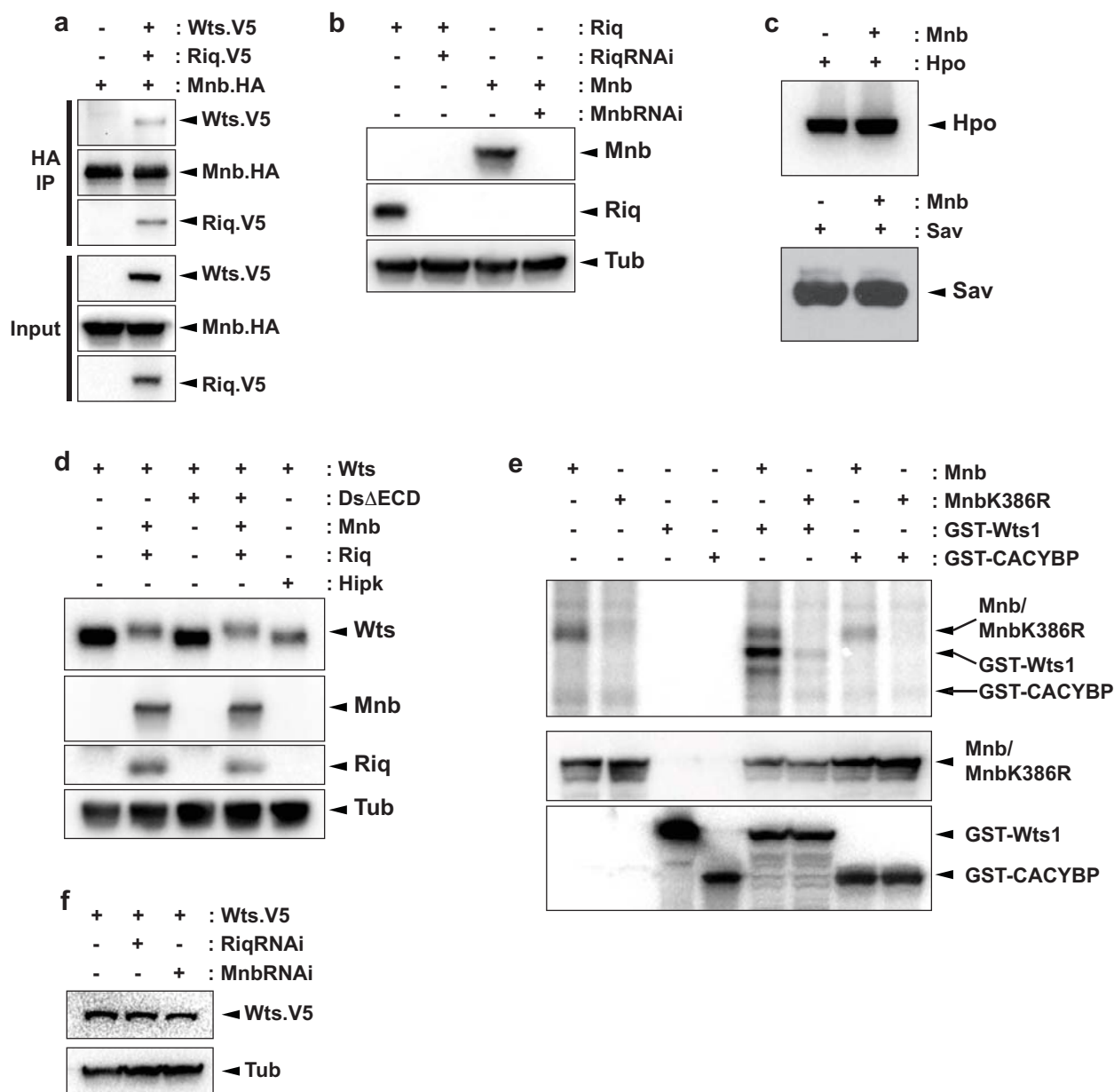


Figure S5 Riquiqui, Minibrain and Warts physically interact with each other and Minibrain phosphorylates Warts. (a) S2 cells were transfected with the indicated plasmids and immunoprecipitations performed using anti-HA antibodies. Subsequently, immunoprecipitates and input lysates were subjected to SDS-PAGE and Western blotted to reveal the indicated proteins. (b-d) Western blot analysis of lysates from S2 cells transfected with the indicated plasmids and Western blotted to reveal the indicated proteins. In (b) Riq or Mnb were expressed in S2 cells in the presence or absence of dsRNA specific for Riq or Mnb, respectively. In (c) Mnb did not induce changes in Hpo or Sav mobility. In (d) Mnb, but not Hipk influenced Wts mobility. (e)

Kinase assays performed using recombinant GST-Wts1 or GST-CACYBP as substrates and either Mnb or Mnb K386R immunoprecipitated from S2 cells. Immunopurified and recombinant proteins were incubated alone or together in kinase buffer containing γ^{32} P-ATP and subjected to SDS-PAGE (upper panel). Western blotting was used to detect input proteins (lower panels). Mnb phosphorylated GST-Wts1 but not the negative control substrate GST-CACYBP. (f) V5-tagged Wts was expressed in the presence or absence of dsRNA specific for Riq or Mnb in S2 cells. Cells were lysed and lysates were immunoblotted using antibodies to V5 and to Tubulin as a loading control. Wts levels were unchanged when Riq or Mnb were depleted from cells by RNAi.

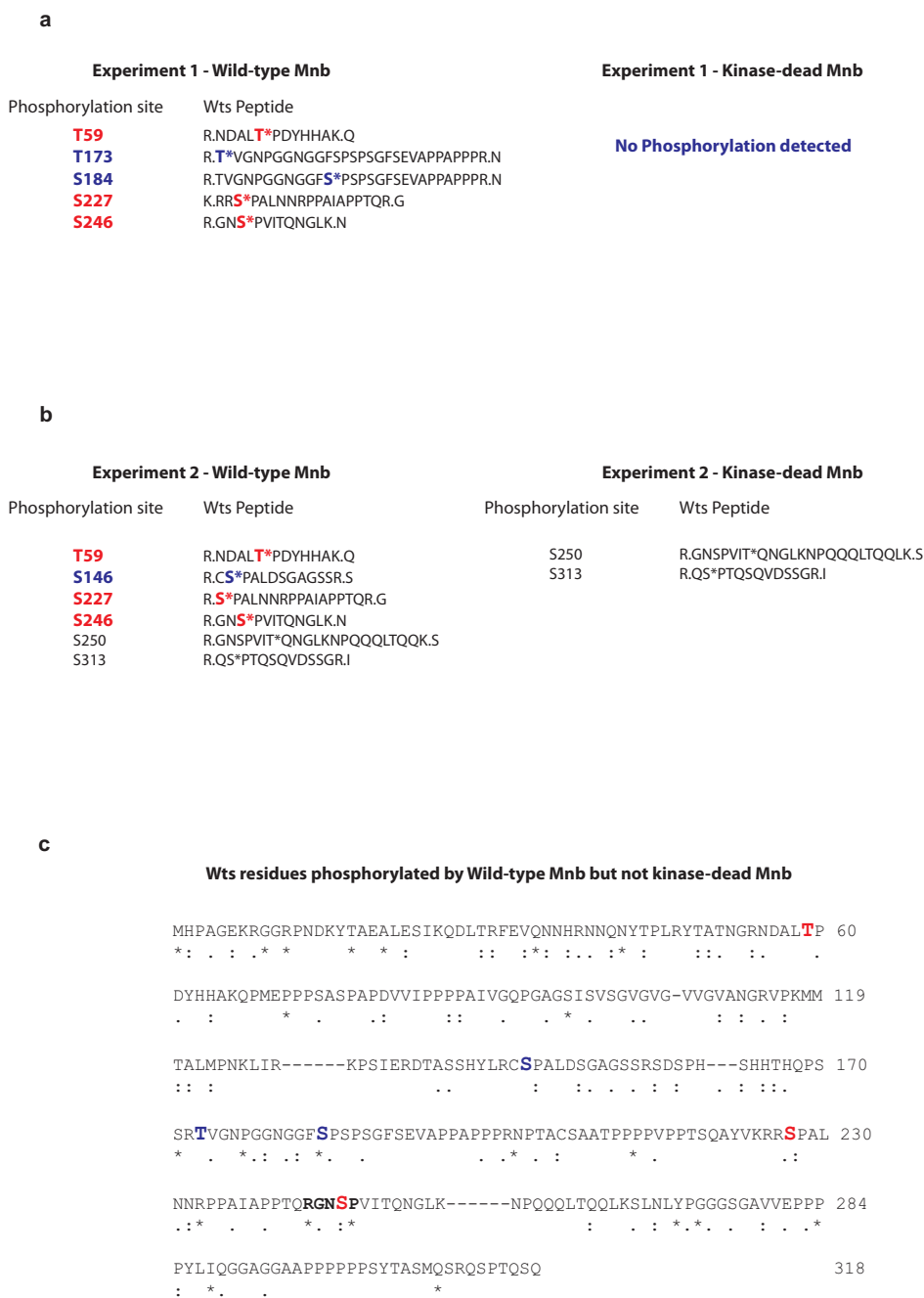


Figure S6 Minibrain phosphorylates six amino acids in the Warts protein, including a DYRK1A consensus site. (a and b) Wts1 (amino acids 1-318 of Wts) peptides that possessed amino acids that were phosphorylated when incubated with either wild-type Mnb or kinase-dead Mnb (Mnb-KD) immunoprecipitates. Experiments 1 and 2 were performed independently and analyzed by different mass spectrometry facilities. In experiment 1, five Wts amino acids were phosphorylated by wild-type Mnb with high confidence, whereas Mnb-KD induced no observable phosphorylation. In experiment 2, six Wts amino acids were phosphorylated by wild-type Mnb with high confidence, whilst two amino acids were phosphorylated in the presence of Mnb-KD. Amino acids that were phosphorylated by Mnb, but not Mnb-KD, are highlighted; amino acids that were phosphorylated in both

independent experiments are red and amino acids that were phosphorylated in only one experiment are blue. (c) A summary of mass spectrometry data outlined in (a) and (b). The amino acid sequence of Wts1 is shown and the degree of conservation with human LATS1, as assessed by CLUSTAL, is indicated below: * indicates perfect conservation, : indicates strongly similar; . indicates weakly similar. As in (a) and (b), amino acids that were phosphorylated in both independent experiments by Mnb, but not Mnb-KD, are highlighted in red and amino acids that were phosphorylated by Mnb in only one experiment are in blue. The Wts sequence that was phosphorylated by Mnb and closely resembles a DYRK1A consensus site (RPXS/TP)² is in bold font. Of note, this site was phosphorylated in each experiment and is conserved between Wts and LATS1.

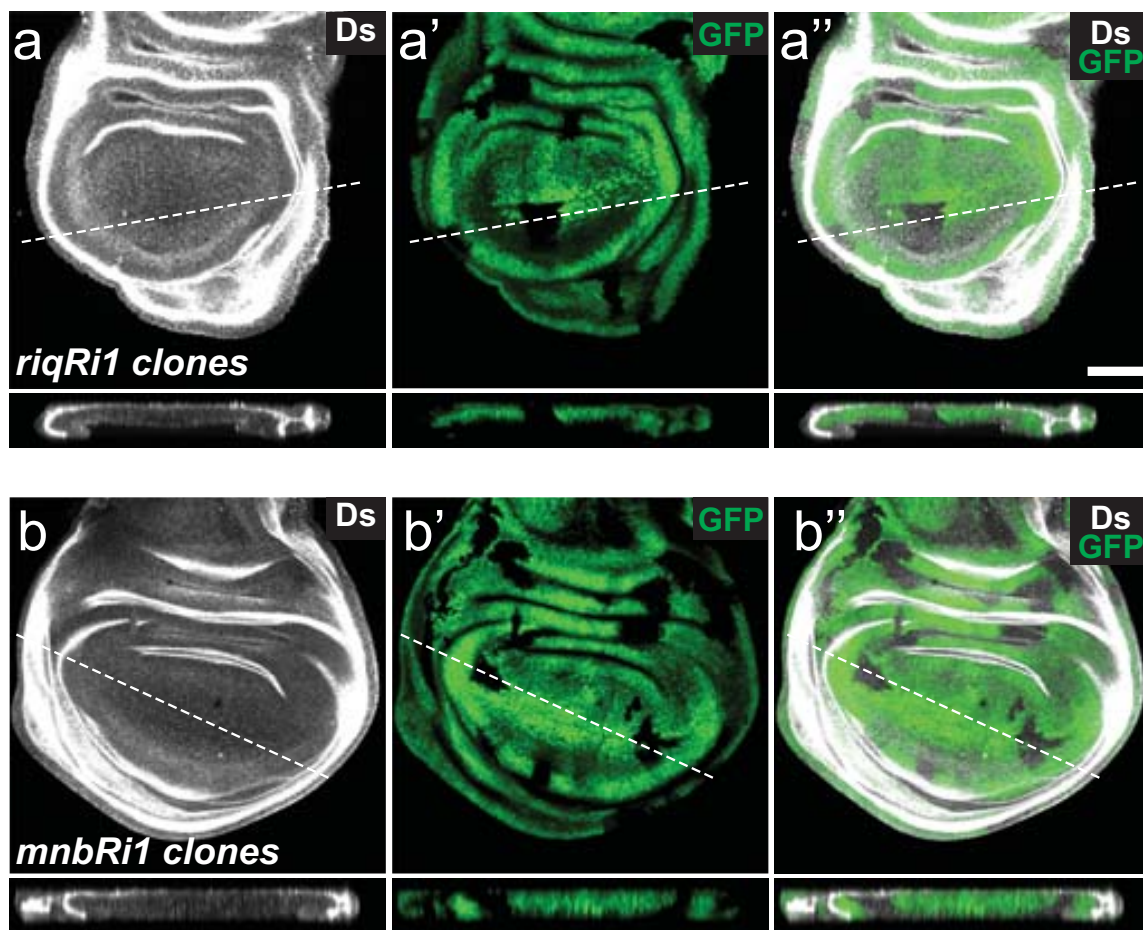


Figure S7 Reduction of Riq or Mnb expression does not affect Dachsous expression. Wing imaginal discs from third instar *D. melanogaster* larvae containing clones of *UAS-riq1* (a) or *UAS-mnb1* (b) were stained for Ds (grey in a and b). Clones were positively marked by co-expression of GFP (a'

and b'). Merged images are shown in (a'' and b''). X-Z sections through the wing pouch are shown below planar sections of wing discs in a-b''. Dashed lines represent the section used to obtain X-Z images. Scale bar represents 50µm.

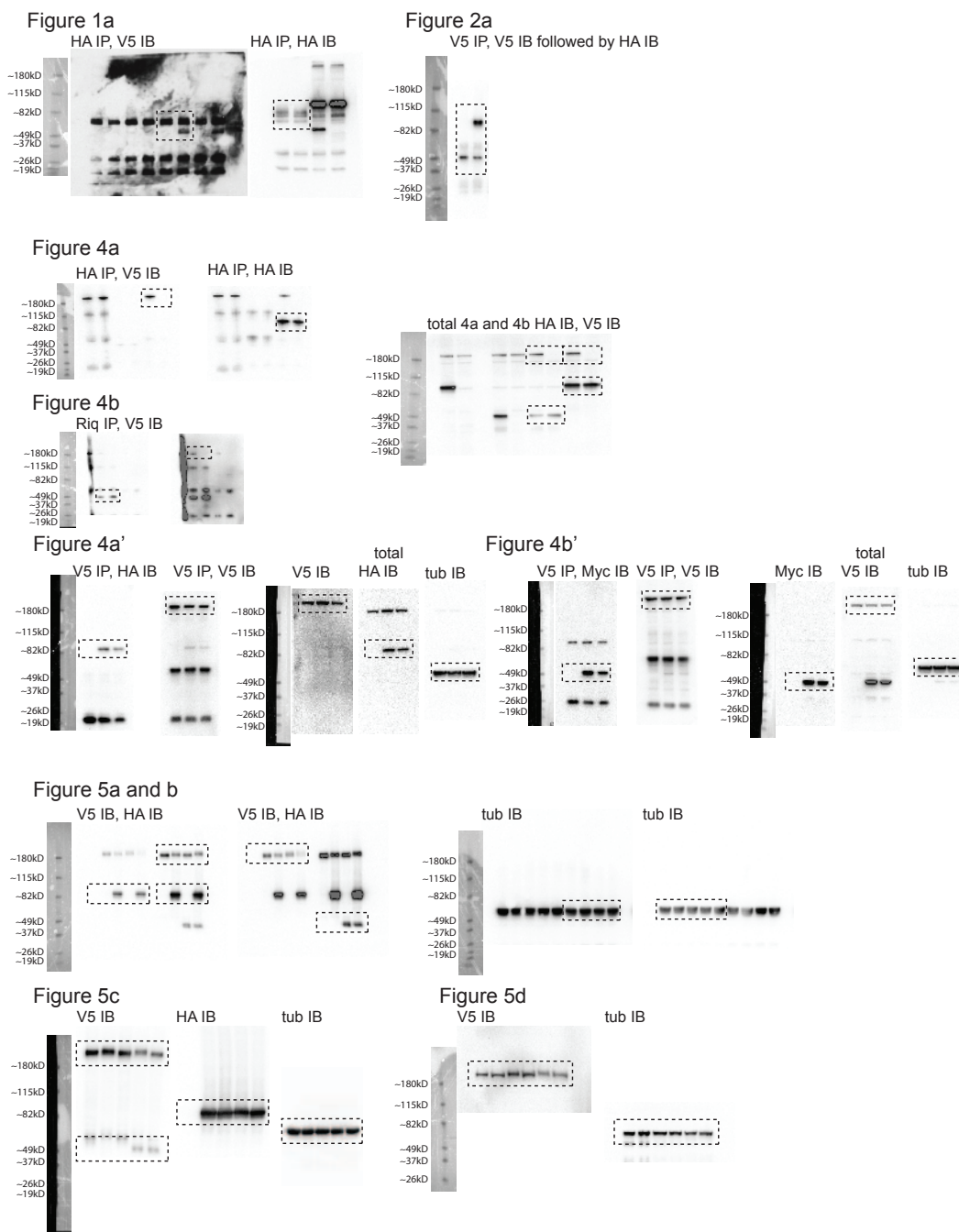
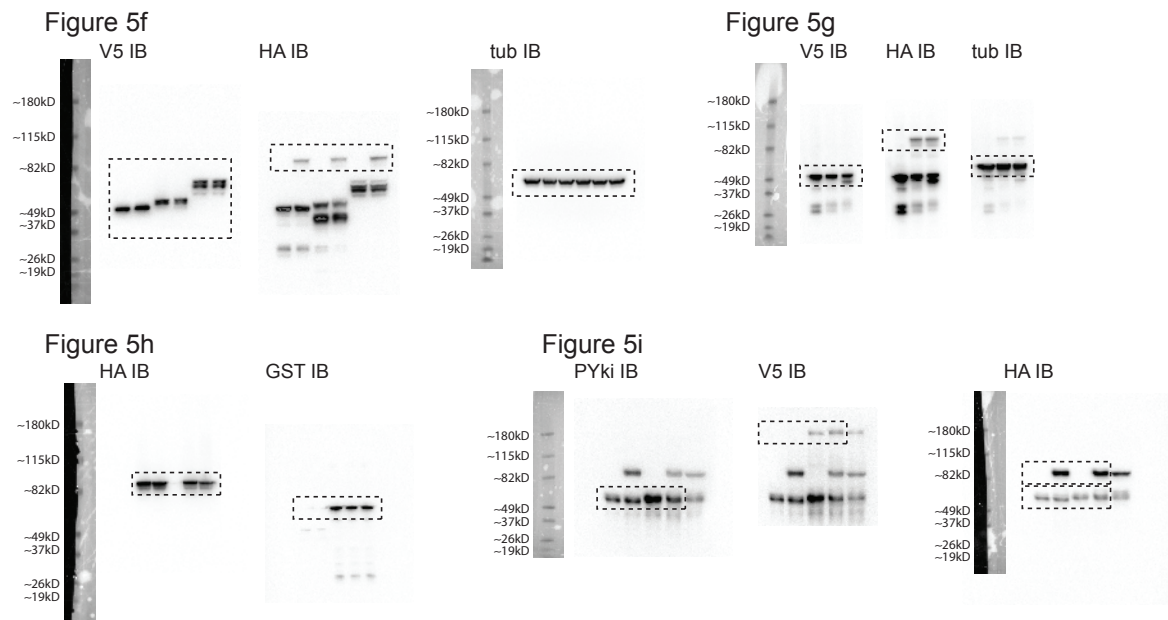


Figure S8 Full scan



Supplementary References

1. Bosveld, F. *et al.* Mechanical control of morphogenesis by Fat/Dachsous/Four-jointed planar cell polarity pathway. *Science* **336**, 724-727 (2012).
2. Himpel, S. *et al.* Specificity determinants of substrate recognition by the protein kinase DYRK1A. *J Biol Chem* **275**, 2431-2438 (2000).